PNAS

Supporting Information for

Activity of estrogen receptor β expressing neurons in the medial amygdala regulates preference towards receptive females in male mice.

Satoshi Takenawa[1], Yutaro Nagasawa[1], Kim Go[1], Yoan Chérasse[2], Seiya Mizuno[3], Kazuhiro Sano[1], and Sonoko Ogawa[1]

[1] Laboratory of Behavioral Neuroendocrinology, University of Tsukuba, Tsukuba, 305-8577, Japan

[2] International Institute for Integrative Sleep Medicine (WPI-IIIS), University of Tsukuba, Tsukuba, Ibaraki 305-8575, Japan.

[3] Laboratory Animal Resource Center and Trans-border Medical Research Center, Institute of Medicine, University of Tsukuba, Tsukuba, Japan.

*Paste corresponding author name(s) here.

Sonoko Ogawa, Ph.D.

Email : ogawa@neurosci.tsukuba.ac.jp

ORCID : 0000-0003-3976-9987

This PDF file includes:

Supporting Information Text

Supplemental Results

Study 1: Additional analysis of Fiber photometry recording of MeApd-ERβ⁺ neuronal activity during preference tests.

During the receptivity-based preference tests (RF vs. XF), male mice showed a preference towards RF stimuli (Fig. 1D and 1E) with paralleled higher MeApd-ERβ⁺ neuronal activity (Fig. 1F and 1G). To demonstrate the relationship between sniffing towards the RF cylinder and MeApd-ERβ⁺ neuronal activity, we showed a representative ΔF/F neuronal activity (%) with behavioral annotations recorded during a RF vs. XF preference test session (Fig. S1A). In addition, representative heat map plots for zFn neuronal activity in each sniffing event during a RF vs. XF (Fig. S1B) and a RF vs. IM (Fig. S1C) preference test recorded in a single mouse are shown. Although overall zFn neuronal activity was higher during RF sniffing events than XF or IM sniffing events, MeApd-ERβ⁺ neurons were not necessarily excited during all RF sniffing events. Therefore, we further analyzed the probability of MeApd-ERβ⁺ neurons being activated in the RF contact area in comparisons to that in the XF or IM contact area. To achieve this, we used the kernel density estimation (KDE) methods with Scott's rule (1).

The KDE analysis visually demonstrated that MeApd-ERβ⁺ neurons had a higher probability of showing enhanced neuronal activity around the RF contact area than that of XF during RF vs. XF preference tests (Fig. S1D and S1E; n=7, $t(6) = 5{,}462$, $p<0.01$** for Fig. S1E). During RF vs. IM preference tests, the KDE analysis also showed that MeApd-ERβ⁺ neurons had a higher probability of exhibiting enhanced neuronal activity in the contact area of RF than that of IM (Fig.S1F and Fig. S1G; n = 7, $t(6) = 7.545$, $p < 0.0001$****; for Fig. S1G). In summary, the KDE analysis graphically demonstrates that MeApd-ERβ⁺ neurons are consistently active around RF in both RF vs. XF and RF vs. IM tests. These results suggest that higher neuronal activity of MeApd-ERβ⁺ cells is associated with the preference of animals for RF stimuli compared to XF or IM stimuli.

Study 2: Additional analysis of responses of MeApd-ERβ⁺ neurons to individually presented social stimuli.

MeApd-ERβ⁺ neuronal activation during sniffing towards the RF cylinder was further confirmed in representative heat map plots of zFn neuronal activity during RF vs. Empty preference tests (Fig. S2A). The KDE analysis showed that the probability of MeApd-ERβ⁺ neurons exhibiting enhanced neuronal activity was higher towards a RF compared to an empty cylinder (Fig. S2B and Fig.S2C; n = 5, $t(4) = 4.693$ $p<0.01$** for Fig. S2C). In XF vs. Empty preference tests, MeApd-ERβ⁺ neurons were also activated during sniffing of the XF cylinder, as shown in representative heat map plots of zFn neuronal activity (Fig. S2D). The KDE analysis visually

showed that the probability of MeApd-ERβ+ neurons exhibiting enhanced neuronal activity was higher in the XF contact area compared to that of an empty cylinder, although it was not statistically significant (Fig. S2E and Fig.S2F, n=5, $t(4) = 1.442$, $p = 0.2226$ for Fig. S2F). Similarly, in preference tests for IM vs. Empty, MeApd-ERβ+ neurons were activated during sniffing towards the IM cylinder (Fig. S2G). Also, the KDE analysis demonstrated that the probability of MeApd-ERβ+ neurons exhibiting enhanced neuronal activity was higher in the IM contact area compared to the empty cylinder (Fig. S2H and Fig. S2I; n = 5, $t(4) = 4.897$, $p<0.01$** for Fig. S2I).

Study 3: Additional data presentation of the effects of DREADD inhibition of MeApd-ERβ+ neurons during preference behavior

During the RF vs. XF tests, we observed that inhibiting MeApd-ERβ+ neuronal activity through CNO injection did not influence the total moving distance in both mCherry- and hM4Di-expressing animals (Fig. S3A; drug x virus, $F_{(2,54)}$ =0. 5852, ns). However, preference towards the RF cylinder was abolished by CNO injection only in the hM4Di group, in terms of time spent in the RF contact area (Fig. S3B; virus x drug x stimulus $F_{(2,54)} = 9.127$ $p<0.001$***, see Table S4 for detailed results of post-hoc analysis), and the time spent sniffing the RF cylinder (Fig. S3C; virus x drug x stimulus $F_{(2,54)} = 6.736$ $p<0.01$**, see Table S4 for detailed results of post-hoc analysis). In contrast, there was no effect of CNO injection on any measures during the RF vs. IM tests, suggesting inhibition of MeApd-ERβ+ neuronal activity did not influence behavior (Fig. S3D, S3E and S3F, Table S4). Note that Fig. S3B, S3C, S3E, and S3F show actual values of the data presented as % values in Fig. 3E, 3F, 3F, and 3I.

Study 4: Supplemental data presentation for viral tracing of MeApd-ERβ+ neurons

To investigate the afferent projections of MeApd-ERβ+ neurons, we used a Cre-dependent viral tracer (Fig. S4A), which specifically labeled the synaptic terminals of these neurons. Across sections ranging from Bregma +0.14 mm to - 3.08 mm, we found that the majority of MeApd-ERβ+ neurons projected to the BNST, while very few projected to the hypothalamus (Fig. S4B). We observed that the synaptic terminals of MeApd-ERβ+ neurons were highly concentrated in the BNSTp (Fig. S4C). In addition, we examined the functional connections between MeApd-ERβ+ neurons and BNSTp in mice injected with AAV for Cre-dependent expression of ChR2 (Fig.S4D). Optogenetic stimulation of the MeApd-ERβ+ neurons (Fig. S4E and S4F) indeed excited downstream BNSTp neurons in ChR2-expressing but not control EYFP-expressing animals, as revealed by the induction of cFos (Fig.S4G and S4H) .

Study 4: Additional data presentation of the effects of DREADD inhibition of MeApd-ERβ+ neurons on preference behavior and BNSTp firing probability.

To investigate the effects of chemogenetic inhibition of MeApd-ERβ$^+$ neurons on the activity of BNSTp neurons, we injected a viral vector that induces GCaMP7f expression non-specifically (see Fig. 4A–4C). The mice were then tested four times as shown in Fig. S5A. To demonstrate the relationship between sniffing towards the RF cylinder and BNSTp neuronal activity, we showed a representative ΔF/F neuronal activity (%) with behavioral annotations recorded during a RF vs. XF preference test session under saline-injected condition (Fig. S5B). Representative heat map plots for zFn neuronal activity in each sniffing event demonstrate that DREADD inhibition of MeApd-ERβ$^+$ neurons by CNO injection decreased BNSTp neuronal activity during sniffing towards the RF cylinder (Fig. S5C). In the RF vs. XF test, as expected, CNO injection disrupted preference towards RF as shown in time spent in the RF contact area (Fig. S5D, drug vs. stimulus, $F_{(1,20)} = 13.64$, $p<0.01$**, RF x XF for Saline $p<0.05$*, for CNO ns), and time spent sniffing towards the RF cylinder (Fig. S5E, drug x stimulus, $F_{(1,20)} = 13.12$, $p<0.01$**, RF vs. XF for Saline $p<0.05$*, for CNO ns). The KDE analysis also revealed that higher probability of BNSTp neurons exhibiting prominent neuronal activity against RF over XF seen in the saline control condition was abolished during preference tests under CNO injection (Fig. S5F and S5G; drug x stimulus $F_{(1,20)} = 23.80$ $p<0.0001$****, RF vs. XF for Saline $p<0.0001$****, for CNO ns, Fig. S5F).

In contrast, DREADD inhibition of MeApd-ERβ$^+$ neurons did not affect the neuronal activity pattern of BNTSp in RF vs. IM tests, as shown in representative heat map plots (Fig. S5H). Male mice spent more time in the RF contact area (Fig. S5I, stimulus $F_{(1,20)} = 10.90$ $p<0.01$**, drug x stimulus ns) and demonstrated longer sniffing time towards the RF cylinder under both saline and CNO injection conditions (Fig. S5J; stimulus $F_{(1,20)} = 10.83$ $p<0.01$**; drug x stimulus ns). The KDE analysis also showed that the probability of the BNSTp neurons exhibiting prominent neuronal activity was higher around the RF contact area than that of the IM in both saline and CNO injection conditions (Fig. S5K and S5L, stimulus $F_{(1,20)} = 20.66$ $p<0.001$***, drug x stimulus ns for Fig. S5K).

Supplemental Study: Effects of optogenetic stimulation of MeApd-ERβ$^+$ neurons on the levels of sniffing behavior

Based on the fiber photometry recordings from MeApd-ERβ$^+$ neurons in Studies 1 and 2, we have hypothesized that activation of MeApd-ERβ$^+$ neurons by sniffing of a specific stimulus, such as RF, may further enhance sniffing towards the same stimulus (i.e., RF), resulting in a preference for RF over XF. To test this hypothesis, we examined whether optogenetic stimulation of MeApd-ERβ$^+$ neurons during sniffing towards a non-preferred stimulus (e.g., XF) might enhance sniffing to that specific stimulus.

We unilaterally injected mice with 300ul of AAV9-hSyn-DIO-ChR2-EYFP or AAV9-hSyn-DIO-ChR2-EYFP (Fig. S6A) and performed a 15-minute RF vs. XF preference test while optogenetically stimulating ChR2-expressing MeApd-ERβ$^+$ neurons only when the mice sniffed

the XF cylinder during the middle 5-minute block (Fig. S6B). As expected, during the first (pre-stimulation) and third (post-stimulation) 5-minute blocks, the mice showed higher levels of sniffing towards RF than XF (Fig. S6C and S6D). However, during the second 5-minute block, by optogenetically stimulating MeApd-ERβ$^+$ neurons, the preference was reversed in the ChR2-expressing group. Further analysis of behavioral changes between the three 5-minute blocks revealed the reversal of preference during the second 5-minute stimulated block, as shown in time spent in the contact area (Fig. S6E, optical stimulation × social stimulus, $F_{(2,24)} = 18.00$ $p < 0.0001$****; RF < XF during the stimulation block, $p<0.001$***), sniffing duration (Fig. S6F ; optical stimulation × social stimulus, $F_{(2,24)} = 10.63$ $p<0.01$**, RF vs. XF during the stimulation block, *ns*), and the number of sniffing events (Fig. S6G, optical stimulation × social stimulus, $F_{(2,24)} = 20.34$ $p <0.0001$****, RF vs. XF for during the stimulation block, $p<0.001$***). However, optical stimulation did not affect sniffing duration per event (Fig. S6H, optical stimulation × social stimulus $F_{(2,24)} = 0.8703$, *ns*).

We also confirmed that preference towards the XF cylinder during optical stimulation was only seen in ChR2-expressing animals but not in the animals injected with the control EYFP virus. The optogenetic activation of MeApd-ERβ$^+$ neurons increased sniffing duration towards the XF cylinder (Fig. S6I, optical stimulation x virus $F_{(2,24)} = 7.673$ $p<0.001$***, ChR2 vs. EYFP for during the stimulation block, $p <0.0001$****) and the number of sniffing events towards the XF cylinder (Fig. S6J, optical stimulation x virus $F_{(2,24)} = 2. 737$ *ns*, ChR2 vs. EYFP for during the stimulation block, $p<0.01$**) only in ChR2-expressing animals. Also, a decrease of the percentage of time sniffing towards the RF cylinder was clearly observed only in ChR2 expressing animals during the optical stimulation (Fig. S6K, optical stimlation x virus $F_{(2,24)} = 3.527$ $p<0.05$*, ChR2 vs. EYFP for during the stimlation block, $p<0.01$**). These findings suggest that optogenetic stimulation of MeApd-ERβ$^+$ neurons during the investigation of non-preferred XF could drive the animal to repeatedly investigate XF and form an artificial preference for it over RF (Fig. S6L).

Supplemental methods

Generation and verification of ERβ-iCre mice

ERβ-iCre mice were generated using the CRISPR-Cas9 system, as described previously (2). A *p2A-iCre rGpA* sequence was inserted on the 5' side of the stop codon of the C57BL/6N mouse *Esr2* gene (Fig. S7A). All animals resulting from the CRISPR-Cas9 method were screened for successful knock-in of *Esr2-iCre*, followed by unintentional random integration of Cas9 expression and donor DNA vectors. The resulting lines were sequenced upstream of the *iCre* gene to confirm the absence of unintentional mutations in the *Esr2* gene. All the primers used are listed in Table S1.

Since ERβ is expressed in neuronal embryonic cells in mice (3, 4), we could not confirm the expression pattern of *iCre* by reporter mouse assays. Instead, we examined *iCre* expression in ERβ-expressing cells by backcrossing ERβ-iCre mice with previously reported ERβ-red fluorescent protein (RFP)-tg mice (5). We injected ERβ-iCre and ERβ-RFP double-positive male mice (n = 3; eight weeks old) with 300 nL of AAV2-hSyn-DIO-green fluorescent protein (GFP) in the MeApd (Fig. S7B) and perfused them two weeks later. Under a fluorescent microscope, we observed the expression of Cre-induced GFP and ERβ-RFP in MeApd (between Bregma -1.56 and -2.04) (Fig. S7C). Out of 2505 GFP-positive cells, 2229 cells (89%) were RFP-positive (Fig. S7D), indicating that Cre was successfully expressed in ERβ-positive cells in the MeApd. Detailed methods are described below.

Animal housing and surgical procedure

Male ERβ-iCre-positive mice with a C57BL/6N background, aged between 10 and 14 weeks at the beginning of each study, were used as experimental animals. Male and female ERβ-iCre-negative mice, aged between 10 and 14 weeks, were used as stimulus animals for preference behavioral tests. All mice were housed under a 12-hour light-dark cycle, with lights turned off at noon, and were provided with food and water available *ad libitum*. All experiments were approved by the Animal Care and Use Committee and the Recombinant DNA Use Committee of the University of Tsukuba and were conducted following the National Institute of Health guidelines. All efforts were made to minimize the number of animals used and their suffering.

All experimental animals were stereotaxically injected with various types of viruses under inhalation anesthesia with 1–3% isoflurane (Pfizer). Virus injections were performed using a Hamilton syringe 7000RN with a custom-made 33-gauge, 45° beveled needle tip connected to a Micro4-injection pump (World Precision Instruments). The injection site coordinates were determined based on the Mouse Brain in Stereotaxic Coordinates (6). Detailed information is provided for each experiment, and all viruses used in this study are listed in Table S2. After surgery, all mice were individually housed in plastic cages (12.5 x 20 x 11 cm). Two weeks after surgery, all mice were screened for baseline preference towards RF against XF using the test

paradigm described below. Mice that failed to show a preference towards the RF were excluded from the study.

A detailed description of the preference test

The preference test apparatus and paradigms were designed based on previous studies conducted in our laboratory (7, 8). In brief, each experimental mouse was placed in a white plastic open field (33 cm × 28 cm) under red or dim light (10 lux), depending on the paradigm, with clean bedding, and tested against a pair of stimulus mice, unless otherwise described. The test duration was either 10 or 15 minutes, as stated in each study. All behavioral tests were performed starting at Zeitgeber time 15.

The stimulus mice were individually placed in a transparent acrylic quarter cylinder (7 cm in base radius, 17 cm in height) with 13 small holes (Φ7 mm) near the bottom 3 cm on the rounded side. Before being used as stimulus mice, they were habituated to the cylinders more than three times. All stimulus female mice (RF and XF) were ovariectomized for more than two weeks before testing, under inhalation anesthesia with 1-3% isoflurane, and group-housed (four mice per cage). RF mice were injected subcutaneously with 1 μg 17β-estradiol (Sigma-Aldrich) in 0.1 mL sesame oil at 48 and 24 hours and 500 μg progesterone (Sigma-Aldrich) in 0.1 mL sesame oil at 4 hours before testing. The IM stimulus mice were single-housed for more than one week before testing.

On the day of the preference tests, pairs of RF and XF mice were used in the receptivity-based test, and pairs of RF and IM mice were used in the sex-based preference test. In both tests, stimuli were presented to singly housed C57BL/6N intact tester males before being used as stimuli for the preference tests. Only pairs in which tester males preferred RF mice over XF or IM mice were used for the preference tests on that day.

At the start of the preference tests, a pair of cylinders, each containing different types of stimulus mice (RF, XR, or IM), was placed at the two diagonal corners. The placement of the cylinders was counterbalanced. For some tests, empty cylinders were also used. All preference tests were recorded with a CCD camera placed 70–120 cm above the open field, depending on the experimental setup. The test mice sniffing behavior was quantified using BORIS (Friard & Gamba, 2016) and DeepLabCut (ver. 2.1.8.2) (Mathis et al., 2018) for Studies 1, 2, and 4, and the automated Ogawa-Type Social Interaction Test System (O'HARA & Co., Ltd.) (8) for Study 3. In both cases, the time spent in the contact area, defined as the area 8 cm from the outer surface of the cylinders, and the cumulative number and duration of sniffing behaviors, defined as nose touches at the perforated parts of the cylinders, were recorded.

Fiber photometry recording and data analysis.

ERβ-iCre positive mice were stereotaxically injected with either 600 nL of AAV9-hSyn-DIO-GCaMP7f at MeApd (unilateral, AP: -1.94 mm, ML: ±2.40 mm, DV: -4.75 mm) for Studies 1 and 2, and non-specific AAV9-hSyn-GCaMP7f at the BNSTp (unilateral, AP: -0.22 mm, ML: ±0.5 mm,

DV: -3.50 mm) for Study 4. After a week of virus injection, a NA.039, Φ230 μm glass optic fiber (RWD Life Science) was inserted 200 μm above the injection site and fixed with resin dental cement (Tokuyama Dental) mixed with carbon black (Sigma-Aldrich). The mice were habituated to the test condition more than three times, including the optic cable connection, for 10 minutes at least three weeks after the last surgery. Fiber photometry recordings were performed during the preference tests under red light using a DORIC fiber photometry system (DORIC Lenses), with a built-in amplifier (10x). The excitation of GCaMP7f was done using a 465-nm light-emitting diode, and a 525-nm emission light was filtered for recording. After the last recording session, all mice that were subjected to fiber photometry recordings were perfused to confirm viral infection and fiber placement, as described below.

The movements of the mouse were recorded using a DORIC camera system (DORIC Lenses) linked to a fiber photometry system. The recorded image data underwent a 4 Hz low-pass filter. Sniffing behavior was annotated using BORIS (9) while body movement was tracked using DeepLabCut (ver. 2.1.8.2) (10) in Python (ver. 3.7.6). All fiber photometry recordings were analyzed based on mouse sniffing behavior. The image data from 2 seconds before and 8 seconds after the onset of sniffing were extracted, converted to dF/F0 (dF = 8 seconds from sniffing onset, F0 = mean signals from 2 seconds before sniffing onset), and normalized to the Z-score (zFn). To demonstrate representative data for all sniffing events from an individual animal (Shown in Fig S1B, S1C, S2A, S2D, S2G, S6C and S6H), these sniffing data were converted into a heat map after Z-score normalization. For calculation of the AUC, we analyzed the positive area (0>=n) of zFn data during 8 seconds episodes of sniffing behavior described above, based on Sherathiya, et al 2021(11).To calculate the AUC, we used SciPy ver. 1.10.1, scipy.integrate.simps on Python (ver. 3.11.3). In addition, for the representative figures shown in Fig. S1A and Fig. S6B, recorded data were converted into dF/F0 data by 60-seconds moving average.

Furthermore, the GCaMP signals with Z ≥1 activity during sniffing behavior were sorted as prominent neuronal activity and further processed for the KDE analysis. The processed fiber photometry data were analyzed and aligned with animal behavioral annotations derived from BORIS and DeepLabCut data using Python (ver. 3.8.1).

For the KDE analysis shown in Fig. S1 and S4, all imaging data were filtered using a 4 Hz low-pass filter and smoothed using a 60-second moving average. The data were then converted to Z-scores, and the XY coordinates of mouse body movements were virtually plotted into a 330 x 280 grid and aligned. To generate a KDE plot based on the aligned XY data, we used the scipy.stats.gaussian_KDE package in Scipy (ver. 1.4.1) and determined the KDE bandwidth selection using Scott's rule (1). To compare the KDE probability between neuronal activity and overall body position, we stacked data across all animals, extracted the body positions accompanied by Z ≤1 neuronal activity, and plotted the KDE on the virtual grid (KDE plot, Z ≤1).

To obtain comparable data for each stimulus, we calculated the KDE score within the contact area of each stimulus and termed it the KDE score.

Chemogenetic manipulation of MeApd-ERβ$^+$ neurons

ERβ-iCre positive mice were stereotaxically injected with either 300 µl of AAV2-hSyn-DIO-hM4Di-mCherry or an AAV2-hSyn-DIO-mCherry control virus bilaterally at the MeApd (AP: -1.94 mm; ML: ±2.40 mm; DV: -4.75 mm) to investigate the chemogenetic inhibition of MeApd- ERβ$^+$ neuronal activity on preference behavior in male mice in either simple behavioral analysis (Study 3) or combined analysis with fiber photometry recording in the BNSTp (Study 4). Starting three weeks after surgery, the mice were habituated to intraperitoneal injections of 0.1 mL saline for three days. They were then treated with either saline (day 1 or 3) or CNO (Sigma-Aldrich) at a dose of 1 mg/kg BW (day 2), 15 minutes prior to the test. After the last behavioral test, the mice were perfused, and viral expression was confirmed by immunohistochemical detection of mCherry protein.

Optogenetic stimulation of MeApd-ERβ$^+$ neurons

ERβ-iCre positive mice were stereotaxically injected with 300 µl of AAV2-EF1α-DIO-ChR2-EFYP in the right MeApd (AP: -1.94 mm; ML: ±2.40 mm; DV: -4.75 mm). After one week, an NA0.50, Φ250-µm plastic fiber was inserted 200 µm above the injection site and fixed with resin dental cement (Tokuyama Dental) mixed with carbon black (Sigma-Aldrich) on the skull. Two weeks later, the mice were habituated for 15 minutes to the test condition, including the optic cable connection, three times prior to the preference test. Optogenetic stimulation was delivered manually using a 473 nm laser (LUCIR Inc.) connected to a pulse generator in 20 Hz bursts (10 ms each). The detailed experimental design is described in Supplemental Study below. Animal sniffing behavior was annotated using BORIS (ver. 8.5) (9), and body movement was tracked using DeepLabCut (Mathis et al., 2018) (ver. 2.1.8.2) in Python (ver. 3.7.6) as described previously. Video recordings during the test sessions were analyzed and aligned with the BORIS and DeepLabCut data using Python (ver. 3.8.1). At the end of all behavioral tests, mice were perfused 90 minutes after a 5-minute optogenetic stimulation (20 seconds of 20 Hz bursts, 40 seconds interval) in their home cage, and the fiber placement was confirmed.

Tissue preparation and immunohistochemistry

The mice were anesthetized with pentobarbital (1 mg/kg) and heparin (1000 units/kg) and transcardially perfused with phosphate-buffered saline followed by 0.1 M phosphate buffer (PB) containing 4% paraformaldehyde. The brains were removed and postfixed overnight at 4 °C, followed by a three-day incubation in 30% sucrose in 0.1 M PB. Samples were frozen in Tissue-Tek O.C.T. compound (Sakura Finetek Japan) and coronally sectioned at 60 µm thickness on a

cryostat (MICROM HM-560 Thermo Fisher Scientific).

To block non-specific binding, free-floating sections were incubated in a blocking buffer containing 10% Block Ace (Morinaga) in 50 mM tris buffered saline (TBS; pH, 7.4) for 30 minutes. After blocking, they were incubated overnight at 4°C with either goat anti-GFP (1:2000; ab#6673, Abcam), chicken anti-RFP (1:2000; ab#205402, Abcam), or rabbit anti-cFos(1:2000; ab#190289, Abcam) in 50 mM TBS with 0.2% Triton X. They were then incubated with either alexa488 anti-goat (1:1000; Jackson Immune Research), alexa594 anti-chicken (1:1000; Jackson Immune Research) or alexa594 anti-rabbit (1:1000; Jackson Immune Research) antibodies in 50 mM TBS with 4′,6-diamidino-2-phenylindole (DAPI).

For viral tracing, additional neuronal nuclei (NeuN) staining was performed using rabbit anti-neuronal nuclei (1:5000; EPR12763, Abcam) with alexa680 anti-rabbit (1:1000; Jackson Immune Research) instead of DAPI staining, using the method described above.

Finally, all sections were mounted on gelatin-coated slides, air-dried, and cover-slipped using Fluoromount-G (Southern Biotechnology Associates).

Image analysis

Using a brightfield-fluorescent combined microscope (BZX-2000, KEYENCE), images of the area of interest identified based on the Mouse Brain in Stereotaxic Coordinates (6)-were captured and stitched at 20x magnification. To quantitatively analyze the number of immunopositive cells, we used Fiji (ver. 1.53h). The captured images were thresholded using Otsu Thresholding (12), then binarized. The resulting binarized signals were automatically counted as positive signals.

Statistical analysis

We used Numpy 1.19.0 for statistical analysis of the fiber photometry and animal movement data derived using Python. All behavioral annotation data obtained by BORIS was statistically analyzed using a student's t-test or an analysis of variance using GraphPad Prism 9. Differences were considered significant at p <0.05*, p <0.01**, p <0.001***. All statistical analyses are summarized in Tables S3 and S4.

Specific methods for studies 1–4 and the supplemental study

Study 1: Fiber photometry recording of MeApd-ERβ$^+$ neuronal activity during preference tests

The neuronal activity of MeApd-ERβ$^+$ during preference tests was recorded using fiber photometry methods for 10 minutes in seven naive ERβ-iCre-positive male mice. Each mouse was tested twice, once for the receptivity-based preference of RF vs. XF and once for the sex-based preference of RF vs. IM, on separate days with a fixed order and one-week intervals between tests. We analyzed preference behavior and neuronal activity during the sniffing towards each stimulus mouse using a custom program developed in Python (ver. 3.8.1) and aligned it with

the animal behavioral annotation derived by BORIS and DeepLabCut (refer to the above for details of each method). Finally, all animals were perfused, and the fiber insertion sites were confirmed under a microscope (Fig. S8).

Study 2: Fiber photometry recording of MeApd-ERβ positive neurons towards individually presented social stimuli

The neuronal activity of MeApd-ERβ$^+$ during preference tests was recorded with fiber photometry methods for 10 minutes in five naive ERβ-iCre-positive male mice. Each mouse was tested three times, in the order of RF vs. Empty, XF vs. Empty, and IM vs. Empty, on separate days with one-week intervals between tests. We analyzed preference behaviors and neuronal activity during the sniffing towards each stimulus using a custom program developed in Python (ver. 3.8.1) and aligned them with the animal behavioral annotation derived by BORIS and DeepLabCut (refer to the above for details of each method). Finally, all animals were perfused, and the fiber insertion sites were confirmed under a microscope (Fig. S9).

Study 3: Effects of DREADD inhibition of MeApd-ERβ$^+$ neurons on the RF vs. XF and RF vs. IM preference tests

A total of 15 naïve ERβ-iCre-positive male mice (eight for hM4Di and seven for the mCherry control) were used in this study. MeApd-ERβ$^+$ neurons were inhibited during a 10-minute preference test using DREADD. All mice were tested for preference of RF vs. XF three times, including a baseline control level with saline injection, a CNO injection, and a recovery period with saline injection at a four- to five-day interval.

They were then tested for preference between RF and IM using the same protocol, starting seven days after the last test for RF vs. XF. For automatic quantification of the sniffing behavior of test mice, the Ogawa-Type Social Interaction Test System, which has been previously described (8) was used to track the nose tip and body movements of the animals (refer to the above for details of each method).

Study 4: Viral tracing of MeApd-ERβ$^+$ neurons

A total of three ERβ-iCre-positive mice were stereotaxically injected with 300 µl of AAV2-Flex-synaptophysin-enhanced GFP into the right MeApd (AP: -1.94 mm, ML: ±2.40 mm, DV: -4.75 mm). After three weeks, the mice were perfused, and viral expression was confirmed by immunohistochemical detection of enhanced GFP protein.

Study 4: Fiber photometry recording of BNSTp in mice with DREADD inhibition of MeApd-ERβ+ neurons.

A total of six naive ERβ-iCre-positive male mice were used in this study. During the preference

tests, the neuronal activity of BNSTp was non-specifically recorded using fiber photometry methods while chemogenetically manipulating the neuronal activity of MeApd-ERβ$^+$.

All mice were subjected to two preference tests for RF vs. XF, one week apart, with saline injection in the first test and CNO injection in the second test. One week after the second test, the mice were tested for their preference for RF vs. IM using the same protocol. We analyzed preference behavior and neuronal activity during the sniffing towards each stimulus mouse using a custom program developed in Python (ver. 3.8.1) and aligned it with the animal behavioral annotation derived by BORIS and DeepLabCut (refer to above for details of each method). Finally, all animals were perfused, and the fiber insertion sites were confirmed under a microscope (Fig. S10).

Supplemental Study: Optogenetic stimulation of MeApd-ERβ$^+$ neurons during the preference test

A total of seven naive ERβ-iCre-positive male mice were used in this study and injected with a AAV expressing ChR2 (n = 7) or EYFP (n = 7). MeApd-ERβ$^+$ neurons were optogenetically activated during preference tests. Each mouse underwent two preference tests for RF vs. XF on consecutive days (days 1 and 2). Mice were tested for baseline preference without and with optogenetic stimulation on days 1 and 2, respectively.

Each preference test was conducted for 15 minutes and divided into three 5-minute blocks: pre-stimulation, stimulation, and post-stimulation. On day 2, optogenetic stimulation was manually delivered during the stimulation block while the animal was sniffing the XF through holes on the rounded side of the cylinder. All behavioral annotations were derived using BORIS, and mouse movements were tracked using DeepLabCut (refer to the above for details of each method). Finally, all animals were perfused, and the fiber insertion sites were confirmed under a microscope (Fig. S11).

Table S1. Primers used for screening ERβ-iCre mice

sequence	description
GTCCCTGGTGATGAGGAGAA	iCre detect F
ATCAGCATTCTCCCACCATC	iCre detect R
TACAGCTTGGTGATGAGGTTTTGCTCTT	EsrCre detect 5F
AGATCCATCTCTCCACCAGCTTGGTAAC	EsrCre detect 5R
ACAGACAGGAGCATCTTCCA	iCre seq R
GAGGATGTGAGGGACTACCTCCTGTACC	EsrCre detect 3F
ACACATTTTGTGAATTTGCCATGTTCCT	EsrCre detect 3R
AGTTCATCAAGCCCATCCTG	Cas9 detection F
GAAGTTTCTGTTGGCGAAGC	Cas9 detection R
TTGCCGGGAAGCTAGAGTAA	Amp detection F
TTTGCCTTCCTGTTTTTGCT	Amp detection R

Table S2. AAV related plasmids used in this study

Plasmid name	Source	Reference
pGp-AAV-syn-jGCaMP7f-WPRE	pGP-AAV-syn-jGCaMP7f-WPRE was a gift from Douglas Kim & GENIE Project (Addgene plasmid # 104488 ; http://n2t.net/addgene:104488 ; RRID:Addgene_104488)	**(10)**
pAAV-hSyn-DIO-EGFP	pAAV-hSyn-DIO-EGFP was a gift from Bryan Roth (Addgene plasmid # 50457 ; http://n2t.net/addgene:50457 ; RRID:Addgene_50457)	unpublished
pAAV-hSyn-DIO-mCherry	pAAV-hSyn-DIO-mCherry was a gift from Bryan Roth (Addgene plasmid # 50459 ; http://n2t.net/addgene:50459 ; RRID:Addgene_50459)	**(11)**
pAAV-hSyn-DIO-hM4D(Gi)-mCherry	pAAV-hSyn-DIO-hM4D(Gi)-mCherry was a gift from Bryan Roth (Addgene plasmid # 44362 ; http://n2t.net/addgene:44362 ; RRID:Addgene_44362)	**(11)**
pAAV-Ef1a-DIO hChR2(E123A)-EYFP	pAAV-Ef1a-DIO hChR2(E123A)-EYFP was a gift from Karl Deisseroth (Addgene plasmid # 35507 ; http://n2t.net/addgene:35507 ; RRID:Addgene_35507)	**(8)**
pAAV-Ef1a-DIO -EYFP	pAAV-Ef1a-DIO EYFP was a gift from Karl Deisseroth (Addgene plasmid # 27056 ; http://n2t.net/addgene:27056 ; RRID:Addgene_27056)	**(8)**
pAAV-FLEX-Synaptophysin-GFP	pAAV FLEX Synaptophysin GFP was a gift from Matthew Nolan (Addgene plasmid # 137188 ; http://n2t.net/addgene:137188 ; RRID:Addgene_137188)	**(12)**

Table S3. Statistical summary for the main figures

Figure(s)	Statistical details
Fig. 1D	Student's t-test n=7, t(6)=5.428, p=0.0016**
Fig. 1E	Student's t-test n=7, t(6)=6.37, p=0.0007***
Fig. 1G	Student's t-test n=7, t(6)=12.57, p<0.0001****
Fig. 1H	Student's t-test n=7, t(6)=1.874, p=0.110
Fig. 1I	Student's t-test n=7, t(6)=3.591, p=0.0115*
Fig. 1K	Student's t-test n=7, t(6)=3.247, p=0.0175*

Figure(s)	Statistical details
Fig. 2A	Student's t-test n=5, t(4)=2.009, p=0.115
Fig. 2B	Student's t-test n=5, t(4)=2.664, p=0.0562
Fig. 2D	Student's t-test n=5, t(4)=3.511, p=0.0123*
Fig. 2E	Student's t-test n=5, t(4)=3.480, p=0.0254*
Fig. 2F	Student's t-test n=5, t(4)=1.308, p=0.2611
Fig. 2H	Student's t-test n=5, t(4)=4.420, p=0.0115*
Fig. 2I	Student's t-test n=5, t(4)=8.642, p=0.001***
Fig. 2J	Student's t-test n=5, t(4)=4.589, p=0.0101*
Fig. 2L	Student's t-test n=5, t(4)=4.897, p=0.0081**

Table S3. Statistical summary for the main figures(continued)

Figure(s)	Statistical details		
Fig. 3E	**Two way-ANOVA**		
	Drug	**Virus**	**Interaction**
	F(2,54)=3.631 p=0.0332**	F(1,54)=10.22 p=0.0023**	F(2, 54)=8.838 p=0.0005***
	post hoc ; Bonferroni's t-test		
	mCherry vs hM4Di	Saline01: ns CNO: mCherry > hM4Di, p<0.0001**** Saline02: ns	
Fig. 3F	**Two way-ANOVA**		
	Drug	**Virus**	**Interaction**
	F(2,54)=2.772 p=0.0714, ns	F(1,54)=10.11 p=0.0024**	F(2, 54)=8.604 p=0.0006***
	post hoc ; Bonferroni's t-test		
	mCherry vs hM4Di	Saline01: CNO: mCherry > hM4Di, p<0.0001**** Saline02: ns	
Fig. 3H	**Two way-ANOVA**		
	Drug	**Virus**	**Interaction**
	F(2,54)=0.1771 p=0.1566, ns	F(1,54)=0.9543 p=0.8382, ns	F(2, 54)=1.919 p=0.3330, ns
Fig. 3I	**Two way-ANOVA**		
	Drug	**Virus**	**Interaction**
	F(2,54)=0.2032 p=0.07570, ns	F(1,54)=0.921 p=0.3464, ns	F(2, 54)=0.2798 p=0.3464, ns

Table S3. Statistical summary for the main figures(continued)

Figure(s)	Statistical details		
Fig. 4F	**Two way-ANOVA**		
	Drug	**Stimulus**	**Interaction**
	F(1,20)=0.3302 p=0.5719, ns	F(1,20)=4.012 p=0.0589, ns	F(1, 20)=19.02 p=0.0003***
	post hoc ; Bonferroni's t-test		
	RF vs XF	Saline: RF>XF, p=0.0004*** CNO:, RF=XF, p=0.2220, ns	
Fig. 4I	**Two way-ANOVA**		
	Drug	**Stimulus**	**Interaction**
	F(1,20)=0.00483 p=0.9454, ns	F(1,20)=20.66 p=0.0002 *** RF>IM	F(1,20)=0.5625 p=0.4620, ns

Table S4. Statistical summary for supplemental figures

Figure(s)	Statistical details
Fig. S1E	Student's t-test n=7, t(6)=5,462, p=0.0016**
Fig. S1G	Student's t-test n=7, t(6)=7.545, p<0.0001****

Figure(s)	Statistical details
Fig. S2C	Student's t-test n=5, t(4)=4.693, p=0.0094**
Fig. S2F	Student's t-test n=5, t(4)=1.442, p=0.2226
Fig. S2I	Student's t-test n=5, t(4)=4.897, p=0.0080**

Figure(s)	Statistical details		
Fig. S3A	**Two way-ANOVA**		
	Drug	**Virus**	**Interaction**
	F(2,54)=0.2032 p=0.07570, ns	F(1,54)=0.921 p=0.3464, ns	F (2, 54) = 0.5852 p=0.5605, ns
Fig. S3B	**Three way-ANOVA**		
	Drug	**Virus**	**Stimulus**
	F(2,54)=0.9966 p=0.3758, ns	F(1,54)=0.1.747 p=0.1918, ns	F(1, 54)=129.3 p<0.0001****
	Interaction		
	Virus x Drug	**Virus x Stimulus**	**Virus x Drug x Stimulus**
	F(2,54)=0.305 p=0.7380, ns	F(2,54)=13.21 p=0.0006***	F(2, 54)=9.127 p=0.0004***
	post hoc ; Bonferroni's t-test		
	RF vs XF	mCherry Saline01: RF>XF, p=0.0001*** mCherry CNO : RF>XF, p<0.0001**** mCherry Saline02: RF>XF, p=0.0003***	
		hM4Di Saline01: RF>XF, p=0.0003*** hM4Di CNO : RF=XF, p>0.999, ns hM4Di Saline01: RF>XF, p=0.0001***	

Table S4. Statistical summary for supplemental figures (continued)

Fig. S3C	**Three way-ANOVA**		
	Drug	**Virus**	**Stimulus**
	F (2, 54) = 0.01634 p=0.9838, ns	F (1, 54) = 77.42 p<0.0001****	F (1, 54) = 0.2533 p=0.6168, ns
	Interaction		
	Virus x Drug	**Virus x Stimulus**	**Virus x Drug x Stimulus**
	F (2, 54) = 0.2086 p=0.8123, ns	F (1, 54) = 8.200 p=0.0060**	F (2, 54) = 6.736 p=0.0024**
	post hoc ; Bonferroni's t-test		
	RF vs XF	mCherry Saline01: RF>XF, p=0.0009*** mCherry CNO : RF>XF, p<0.0001**** mCherry Saline02: RF>XF, p=0.0822, ns	
		hM4Di Saline01: RF>XF, p=0.0036** hM4Di CNO : RF=XF, p>0.999, ns hM4Di Saline01: RF>XF, p=0.0114*	
Fig. S3D	**Two way-ANOVA**		
	Drug	**Virus**	**Interaction**
	F (2, 54) = 0.8259 p=0.4433, ns	F (2, 54) = 0.2606 p=0.7715, ns	F (2, 54) = 0.8259 p=0.2365, ns
Fig. S3E	**Three way-ANOVA**		
	Drug	**Virus**	**Stimulus**
	F (2, 54) = 4.962 p=0.0105*	F (1, 54) = 0.1852 p=0.6687, ns	F (1, 54) = 93.77 p<0.0001****
	Interaction		
	Virus x Drug	**Virus x Stimulus**	**Virus x Drug x Stimulus**
	F (2, 54) = 1.837 p=0.1691, ns	F (1, 54) = 0.5112 p=0.4777, ns	F (2, 54) = 1.307 p=0.2789, ns
Fig. S3F	**Three way-ANOVA**		
	Drug	**Virus**	**Stimulus**
	F (2, 54) = 3.473 p=0.0381*	F (1, 54) = 6.463 p=0.0139*	F (1, 54) = 34.98 p<0.0001****
	Interaction		
	Virus x Drug	**Virus x Stimulus**	**Virus x Drug x Stimulus**
	F (2, 54) = 1.559 p=0.2197, ns	F (1, 54) = 2.095 p=0.1535, ns	F (2, 54) = 0.4716 p=0.6265, ns

Table S4. Statistical summary for supplemental figures (continued)

Figure(s)	Statistical details		
Fig. S5D	**Two way-ANOVA**		
	Drug	**Stimulus**	**Interaction**
	F (1, 20) = 0.2869 p=0.5981, ns	F (1, 20) = 0.5736 p=0.4577, ns	F (1, 20) = 13.64 p=0.0014**
	post hoc ; Bonferroni's t-test		
	RF vs XF	Saline: RF>XF, p=0.0341* CNO: RF=XF, p>0.999, ns	
Fig. S5E	**Two way-ANOVA**		
	Drug	**Stimulus**	**Interaction**
	F (1, 20) = 1.068 p=0.3138, ns	F (1, 20) = 1.678 p=0.2100, ns	F (1, 20) = 13.12 p=0.0017**
	post hoc ; Bonferroni's t-test		
	RF vs XF	Saline: RF>XF, p=0.0127* CNO: p=0.6331, ns	
Fig. S5F	**Two way-ANOVA**		
	Drug	**Stimulus**	**Interaction**
	F (1, 20) = 0.1039 p=0.7505, ns	F (1, 20) = 13.10 p=0.0017**	F (1, 20) = 23.80 p<0.0001****
	post hoc ; Bonferroni's t-test		
	RF vs XF	Saline: RF>XF, p<0.0001**** CNO: RF=XF, p=0.1826, ns	
Fig. S5I	**Two way-ANOVA**		
	Drug	**Stimulus**	**Interaction**
	F (1, 20) = 0.0003452 p=0.9954, ns	F (1, 20) = 10.90 p=0.0036**	F (1, 20) = 2.376 p=0.1389, ns
Fig. S5J	**Two way-ANOVA**		
	Drug	**Stimulus**	**Interaction**
	F (1, 20) = 2.376 p=0.0002***	F (1, 20) = 10.83 p=0.0037**	F (1, 20) = 0.6485 p=0.4301
Fig. S5K	**Two way-ANOVA**		
	Drug	**Stimulus**	**Interaction**
	F (1, 20) = 0.0.5625 p=0.4620, ns	F (1, 20) = 20.66 p=0.0002***	F (1, 20) = 0.004815 p=0.9454, ns

Table S4. Statistical summary for supplemental figures (continued)

Figure(s)	Statistical details		
Fig. S6E	**Two way-ANOVA**		
	Optical stimulation	**Stimulus**	**Interaction**
	F (2, 24) = 1.244 p=0.3063, ns	F (1, 12) = 0.1471 p=0.7080, ns	F (2, 24) = 18.00 p<0.0001****
	post hoc ; Bonferroni's t-test		
	RF vs XF	pre Stimulation: ns Stimulation: RF<XF, p=0.0004*** post Stimulation: ns	
Fig. S6F	**Two way-ANOVA**		
	Optical stimulation	**Stimulus**	**Interaction**
	F (2, 24) = 0.04482 p=0.9562, ns	F (1, 12) = 0.6118 p=0.4493, ns	F (2, 24) = 10.63 p=0.0005***
	post hoc ; Bonferroni's t-test		
	RF vs XF	pre Stimulation: ns Stimulation: ns post Stimulation: ns	
Fig. S6G	**Two way-ANOVA**		
	Optical stimulation	**Stimulus**	**Interaction**
	F (2, 24) = 2.228 p=0.1296, ns	F (1, 12) = 1.758 p=0.2096, ns	F (2, 24) = 20.34 p<0.0001****
	post hoc ; Bonferroni's t-test		
	RF vs XF	pre Stimulation: ns Stimulation: RF<XF, p=0.0003*** post Stimulation: ns	
Fig. S6H	**Two way-ANOVA**		
	Optical stimulation	**Stimulus**	**Interaction**
	F (2, 24) = 0.08042 p=0.9230, ns	F (1, 12) = 3.076 p=0.1049, ns	F (2, 24) = 0.8703 p=0.4316, ns

Table S4. Statistical summary for supplemental figures (continued)

Fig. S6I	**Two way-ANOVA**		
	Optical stimulation	**Virus**	**Interaction**
	F (2, 24) = 13.86 p<0.0001****	F (1, 12) = 10.87 p=0.0064**	F (2, 24) = 7.673 p=0.0027**
	post hoc ; Bonferroni's t-test		
	EYFP vs ChR2	pre Stimulation: EYFP=ChR2, p>0.999, ns Stimulation: EYFP<ChR2, p<0.0001**** post Stimulation: EYFP=ChR2, p>0.999, ns	
Fig. S6J	**Two way-ANOVA**		
	Optical stimulation	**Virus**	**Interaction**
	F (2, 24) = 2.737 p=0.0850, ns	F (1, 12) = 6.466 p=0.0258**	F (2, 24) = 20.36 p<0.0001****
	post hoc ; Bonferroni's t-test		
	EYFP vs ChR2	pre Stimulation: EYFP=ChR2, p=0.7974, ns Stimulation: EYFP<ChR2, p=0.0060** pre Stimulation: EYFP=ChR2, p=0.1949, ns	
Fig. S6K	**Two way-ANOVA**		
	Optical stimulation	**Virus**	**Interaction**
	F (2, 24) = 6.449 p=0.0057*	F (1, 12) = 6.018 p=0.0304**	F (2, 24) = 3.527 p=0.0454*
	post hoc ; Bonferroni's t-test		
	EYFP vs ChR2	pre Stimulation: EYFP=ChR2, p>0.999, ns Stimulation: EYFP>ChR2, p=0.0049** pre Stimulation: EYFP=ChR2, p=0.7838, ns	

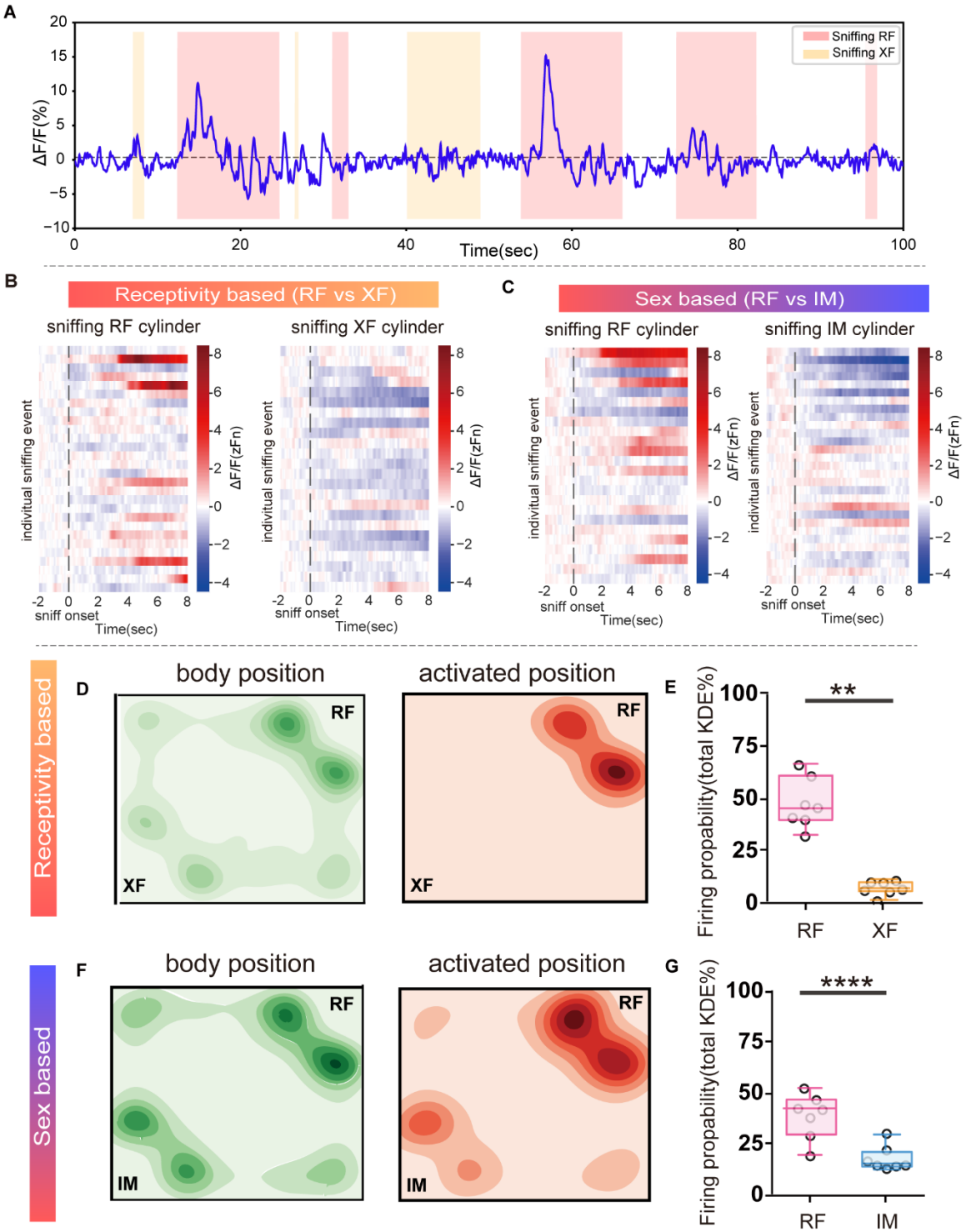
A
Sniffing RF
Sniffing XF
ΔF/F(%)
Time(sec)
B
Receptivity based (RF vs XF)
sniffing RF cylinder
sniffing XF cylinder
indivitual sniffing event
sniff onset
Time(sec)
ΔF/F(zFn)
C
Sex based (RF vs IM)
sniffing RF cylinder
sniffing IM cylinder
Receptivity based
D
body position
activated position
RF
XF
E
Firing propability(total KDE%)
**
RF
XF
Sex based
F
body position
activated position
RF
IM
G
Firing propability(total KDE%)
****
RF
IM

Figure S1. Supplemental figures for Study 1

(A) Representative ΔF/F neuronal activity (%) for 100 seconds from a RF vs. XF preference test session.

(B) Representative zFn neuronal activity from a RF (left) vs. XF (right) preference test session. All sniffing events (2 seconds before and 8 seconds after sniffing onset) are stacked vertically, and neuronal activity is visually demonstrated as a heat map. Red indicates increased neuronal activity, and blue indicates decreased neuronal activity.

(C) Representative zFn neuronal activity from a RF (left) vs. IM (right) preference test session. All sniffing events (2 seconds before and 8 seconds after sniffing onset) are stacked vertically, and neuronal activity is visually demonstrated as a heat map. Red indicates increased neuronal activity, and blue indicates decreased neuronal activity.

(D) Visualization of Kernel Density Estimation (KDE) in RF vs. XF tests, shown in a virtual test environment (RF: top right corner, XF bottom left corner). KDE was derived from body positions (green, left) and positions with Z > 1 GCaMP7f signals (red, right) recorded in 7 animals.

(E) Mean KDE probability score of Z > 1 GCaMP7f signals obtained by summarizing KDE scores in each contact area in RF (red) vs. XF(orange) preference tests (Mean ± SEM, n=7, **; $p<0.01$).

(F) Visualization of KDE in RF vs IM preference tests, shown in a virtual test environment (RF: top right corner, IM bottom left corner). KDE was derived from body positions (green, left) and positions with Z > 1 GCaMP7f signals (red, right) recorded in 7 animals.

(G) Mean KDE probability score of Z > 1 GCaMP7f signals obtained by summarizing KDE scores in each contact area in RF (red) vs IM (blue) preference tests (Mean ± SEM, n=7, ****; $p<0.0001$).

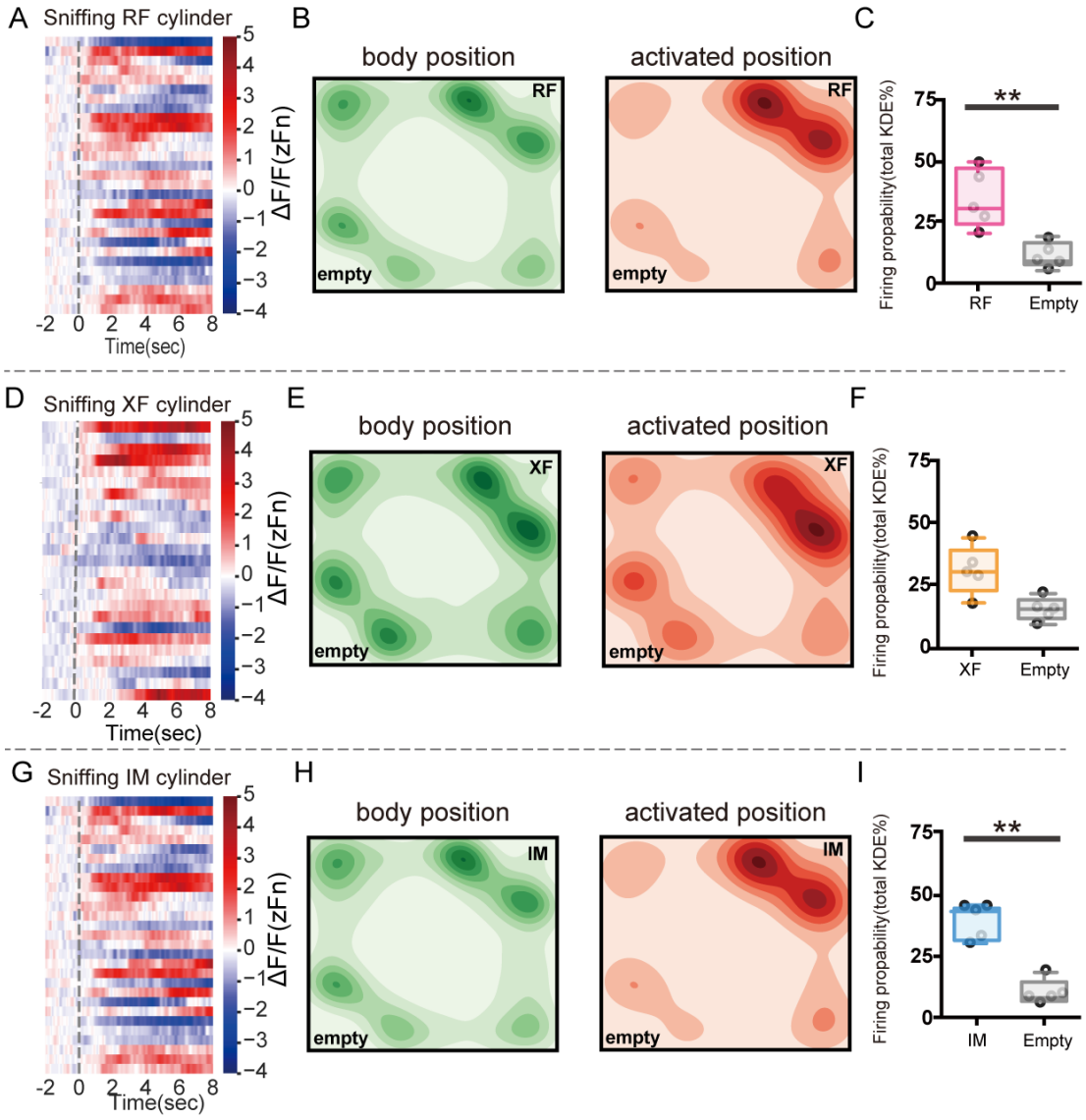
A
Sniffing RF cylinder
ΔF/F(zFn)
Time(sec)
B
body position
activated position
RF
empty
C
Firing propability(total KDE%)
**
RF
Empty
D
Sniffing XF cylinder
E
F
XF
G
Sniffing IM cylinder
H
I
IM

Figure S2. Supplemental figures for Study 2

(A) Representative zFn neuronal activity from a RF vs. Empty preference test session. All sniffing events (2 seconds before and 8 seconds after sniffing onset) are stacked vertically, and neuronal activity is visually demonstrated as a heat map. Red indicates increased neuronal activity, and blue indicates decreased neuronal activity.

(B) Visualization of KDE in RF vs. Empty preference tests, shown in a virtual test environment (RF: top right corner, Empty bottom left corner). KDE was derived from body positions (green, left) and positions with Z > 1 GCaMP7f signals (red, right) recorded in 7 animals.

(C) Mean KDE probability score of Z > 1 GCaMP7f signals obtained by summarizing KDE scores in each contact area in RF (red) vs Empty (gray) preference tests (Mean ± SEM, n=5, **; $p<0.01$).

(D) Representative zFn neuronal activity during a XF vs. Empty preference test session. All sniffing events (2 seconds before and 8 seconds after sniffing onset) are stacked vertically, and neuronal activity is visually demonstrated as a heat map. Red indicates increased neuronal activity, and blue indicates decreased neuronal activity.

(E) Visualization of KDE in XF vs. Empty test shown in a virtual test environment t (XF: right corner, Empty bottom left corner). KDE was derived from body positions (green, left) and positions with Z > 1 GCaMP7f signals (red, right) recorded in 5 animals.

(F) Mean KDE probability score of Z > 1 GCaMP7f signals obtained by summarizing KDE scores in each contact area in XF (orange) vs. Empty (gray) tests (Mean ± SEM, n=5).

(G) Representative zFn neuronal activity during a IM vs. Empty preference test session. All sniffing events (2 seconds before and 8 seconds after sniffing onset) are stacked vertically, and neuronal activity is visually demonstrated as a heat map. Red indicates increased neuronal activity, and blue indicates decreased neuronal activity.

(H) Visualization of KDE in IM vs. Empty test shown in a virtual test environment (IM: top right corner, Empty bottom left corner). KDE was derived from body positions (green, left) and positions with Z > 1 GCaMP7f signals (red, light) recorded in 5 animals.

(I) Mean KDE probability score of Z > 1 GCaMP7f signals obtained by summarizing KDE scores in each contact area in IM (blue) vs. Empty (gray) tests, (Mean ± SEM, n=5, **; $p<0.01$)

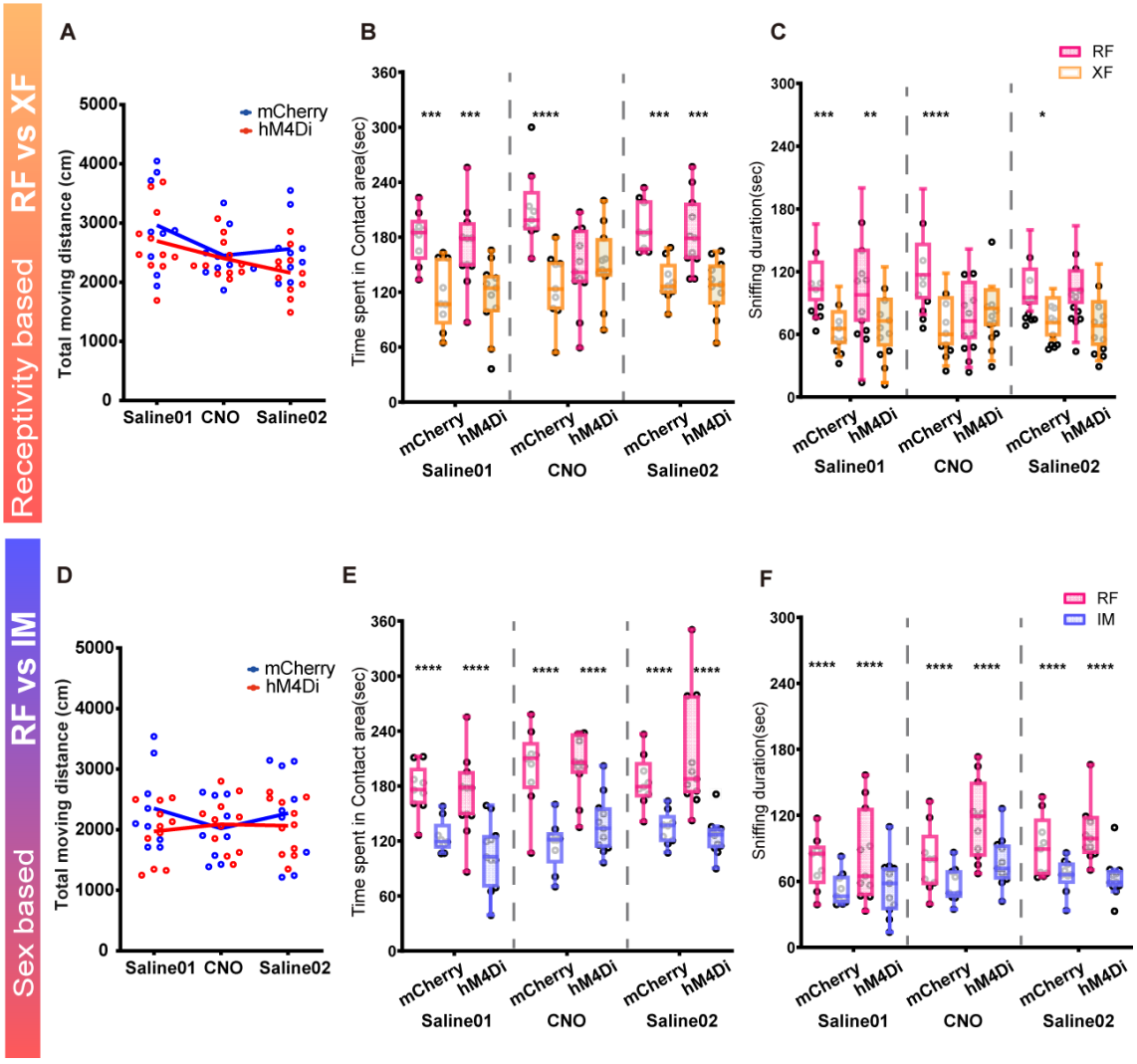
Receptivity based
RF vs XF
A
B
C
mCherry
hM4Di
Total moving distance (cm)
Saline01 CNO Saline02
Time spent in Contact area(sec)
Sniffing duration(sec)
RF
XF
Sex based
RF vs IM
D
E
F
IM

Figure S3. Supplemental figures for Study 3

(A) Mean total moving distance during RF vs. XF preference tests for the hM4Di (red) and mCherry control (blue) AAV injected groups (Mean ± SEM, n = 11 for hM4Di and n = 9 for mCherry control).

(B) Mean time spent in each contact area during RF (red) vs. XF (orange) preference tests for the hM4Di and mCherry control groups. (Mean ± SEM, n = 11 for hM4Di and n = 9 for mCherry control, ***; p <0.001, ****; p <0.0001, RF vs. XF).

(C) Mean time spent sniffing towards each cylinder during RF (red) vs. XF (orange) preference tests for hM4Di (red) and mCherry control (blue) groups. (Mean ± SEM, n = 11 for hM4Di and n = 9 for mCherry control, * ;p <0.05, ** ;p <0.01, *** ;p <0.001, ****; p <0.0001, RF vs. XF).

(D) Mean total moving distance during RF vs. IM preference tests for the hM4Di (red) and mCherry control (blue) AAV injected groups (Mean ± SEM, n = 11 for hM4Di and n = 9 for mCherry control).

(E) Mean time spent in each contact area during RF vs. IM preference tests for the hM4Di (red) and mCherry control (blue) groups. (Mean ± SEM, n = 11 for hM4Di and n = 9 for mCherry control, Main effect of stimulus,****;p <0.0001, RF vs. IM).

(F) Mean time spent sniffing towards each cylinder during RF vs. IM preference tests for the hM4Di (red) and mCherry control (blue) groups. (Mean ± SEM, n = 11 for hM4Di and n = 9 for mCherry control, Main effect of stimulus,****;p <0.0001, RF vs. IM).

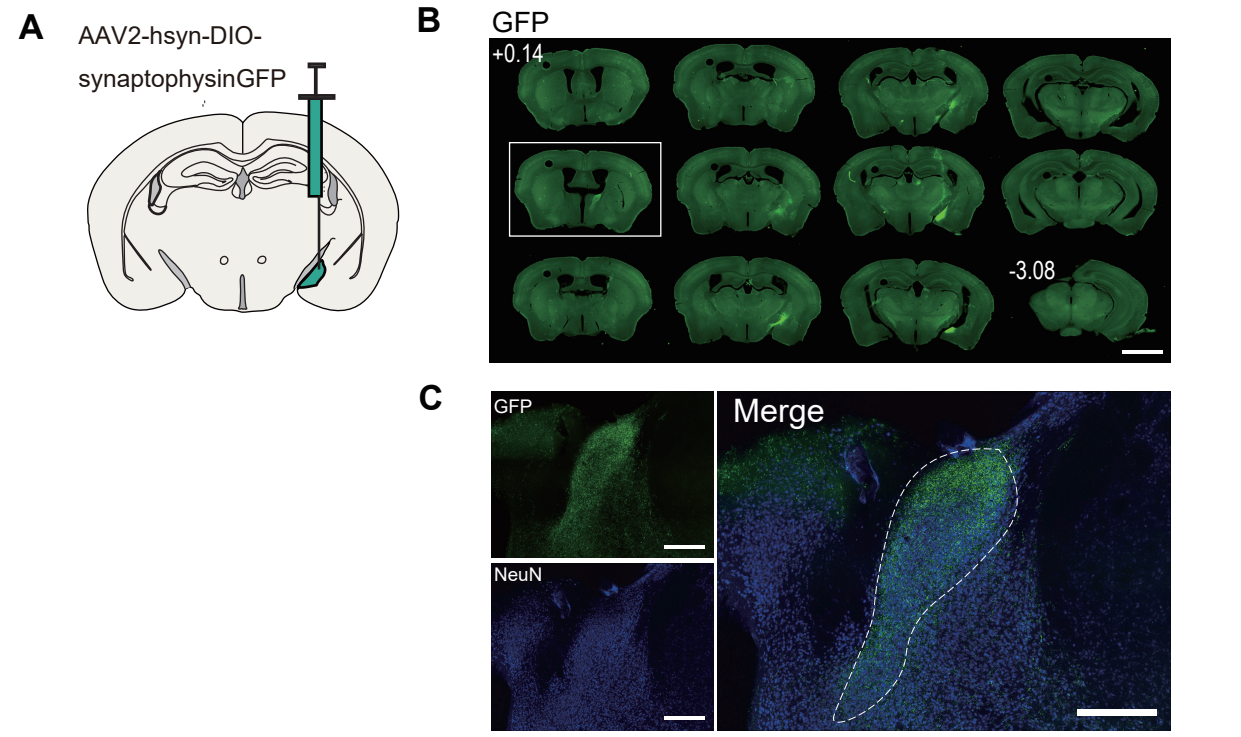
A
AAV2-hsyn-DIO-
synaptophysinGFP
B
GFP
+0.14
-3.08
C
GFP
NeuN
Merge
D
AAV-hSyn-DIO-
ChR2-EYFP
ERβ-iCre mouse
E
Optogenetic stimlulation
in home cage
5min
5min
90min
Start
Light
Stimulation
perfusion
F
ChR2-EYFP
G
EYFP control
ChR2 stimulation
cFos (RED)
cFos (RED)
H
number of cFos positive cells
200
150
100
50
EYFP
ChR2
0.02
-0.10
-0.22
0.02
-0.10
-0.22
from Bragma(mm)

Figure S4. Supplemental figures for Study 4: Viral tracing of MeApd-ERβ$^+$ neurons

(A) Schematic diagram of unilateral AAV injection for tracing MeApd-ERβ$^+$ neurons.

(B) Representative low magnification image showing terminals of MeApd-ERβ$^+$ neurons detected by GFP-tagged synaptophysin across Bregma 0.14mm to -3.08mm (0.24mm intervals). High magnification images for the section in a box are shown in (C). (scale bar = 2.5mm).

(C) Representative image showing terminals of MeApd-ERβ$^+$ neurons detected by GFP-tagged synaptophysin in the BNSTp neurons. Left top: GFP-tagged synaptophysin, left bottom: NeuN, right: merged image. (scale bar = 500um).

(D) Schematic diagram of unilateral AAV injection for optogenetic stimulation of MeApd-ERβ$^+$ neurons.

(E) Timeline to examine cFos induction by optogenetic stimulation of MeApd-ERβ$^+$ neurons.

(F) Representative image of MeApd-ERβ$^+$ neurons expressing ChR2-EYFP (green, scale bar = 500um)

(G) Representative image of cFos positive cells in the BNSTp in EYFP control (left) and ChR2 (right) expressing animals (red: cFos, blue: DAPI; scale bar = 500um).

(H) Mean number of cFos positive cells in three BNSTp sections (Bregma +0.02, -0.10, and -0.22mm) in EYFP (gray) and ChR2 (blue) expressing animals.

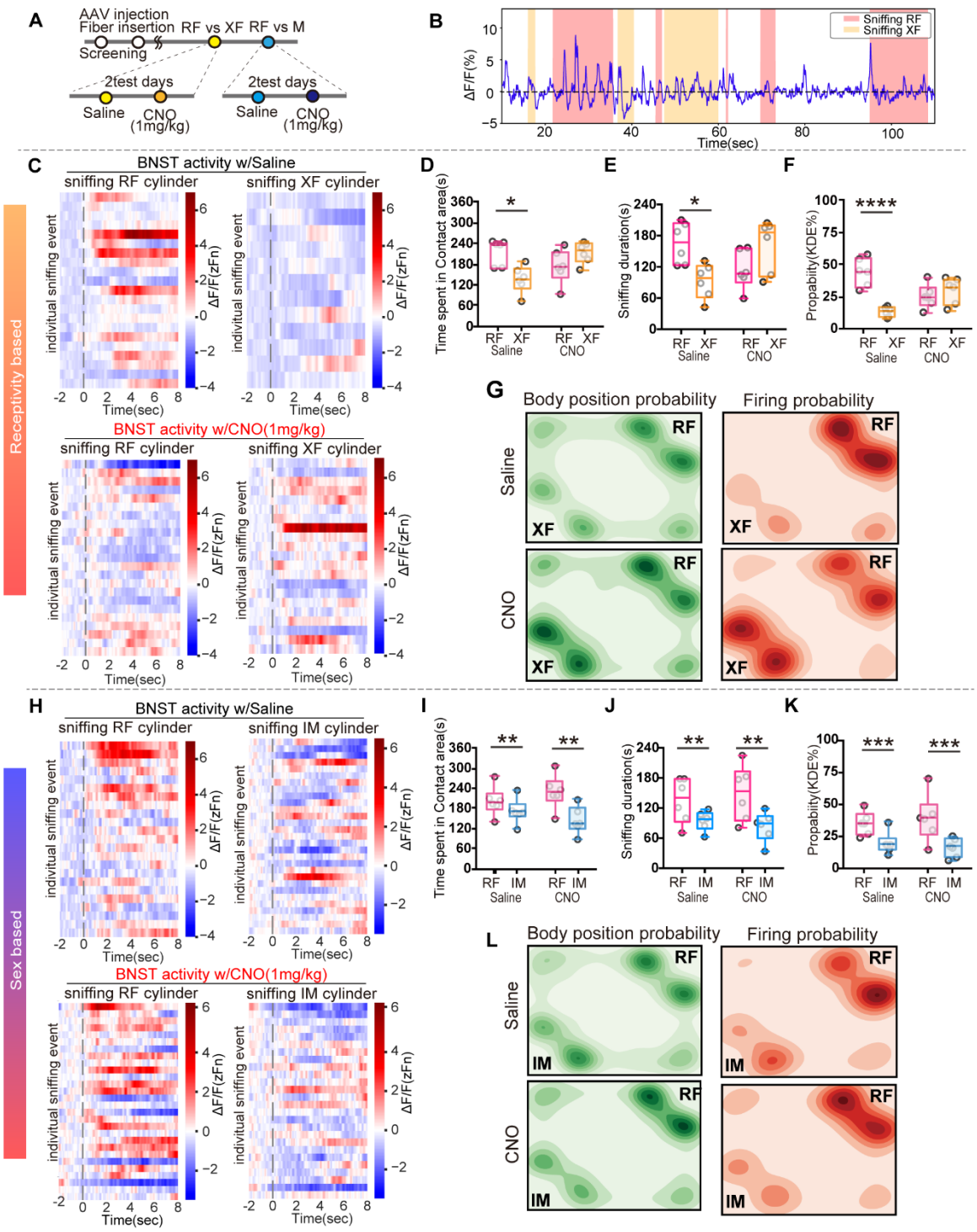
A
AAV injection
Fiber insertion
Screening
RF vs XF
RF vs M
2test days
Saline
CNO (1mg/kg)
2test days
Saline
CNO (1mg/kg)
B
Sniffing RF
Sniffing XF
ΔF/F(%)
Time(sec)
C
BNST activity w/Saline
sniffing RF cylinder
sniffing XF cylinder
indivitual sniffing event
ΔF/F(zFn)
Time(sec)
BNST activity w/CNO(1mg/kg)
Receptivity based
D
Time spent in Contact area(s)
E
Sniffing duration(s)
F
Propability(KDE%)
RF XF
Saline
CNO
G
Body position probability
Firing probability
Saline
CNO
RF
XF
H
BNST activity w/Saline
sniffing RF cylinder
sniffing IM cylinder
BNST activity w/CNO(1mg/kg)
Sex based
I
J
K
L
Body position probability
Firing probability
IM

Figure S5. Supplemental figures for Study 4: Effects of DREADD inhibition of MeApd-ERβ$^+$ neurons on preference behavior and BNSTp firing probability

(A) Timeline for preference tests with DREADD inhibition of MeApd-ERβ$^+$ neuronal activity. Male mice were injected with AAV, and subjected to two preference tests for RF vs. XF (one week apart) with saline (day 1) and CNO (1 mg/kg; day 2) injections. One week after the second test, the mice were tested for their preference for RF vs. IM using the same protocol.

(B) Representative ΔF/F neuronal activity (%) of BNSTp neurons for 120 seconds from a RF vs. XF preference test session.

(C) Representative zFn neuronal activity during a RF (left) vs. XF (right) preference test session under saline (top) or CNO (bottom) injected conditions. All sniffing events (2 seconds before and 8 seconds after sniffing onset) are stacked vertically, and neuronal activity is visually demonstrated as a heat map. Red indicates increased neuronal activity, and blue indicates decreased neuronal activity.

(D) Duration of time spent in each contact area (seconds) during RF (red) vs. XF(orange) preference tests with saline and CNO injection. (Mean ± SEM, n =6, *; p<0.05, RF vs. XF)

(E) Sniffing duration towards each stimulus (seconds) during RF (red) vs. XF(orange) Sniffing duration towards each stimulus (seconds) tests with saline and CNO injection. (Mean ± SEM, n =6, *; p<0.05, RF vs. XF)

(F) Mean KDE probability of Z > 1 GCaMP7f signals obtained by summarizing KDE scores in each contact area during RF (red) vs. XF(orange) preference tests (Mean ± SEM, n =6, ****; p<0.0001, RF vs. XF)

(G) Visualization of KDE shown in virtual test environment (RF: top right corner, XF: bottom left corner). KDE was derived from body positions (green, left) and positions with Z > 1 GCaMP7f signals (red, right) recorded in 6 animals. The upper row represents KDE in saline injection, and the bottom row represents KDE in CNO injection.

(H) Representative zFn neuronal activity during a RF (left) vs. IM (right) preference test session under saline (top) or CNO (bottom) injected conditions. All sniffing events (2 seconds before and 8 seconds after sniffing onset) are stacked vertically, and neuronal activity is visually demonstrated as a heat map. Red indicates increased neuronal activity, and blue indicates decreased neuronal activity.

(I) Duration of time spent in each contact area (seconds) during RF (red) vs. IM(blue) preference tests in saline and CNO injection (Mean ± SEM, n = 6 Main effect of stimulus, **; p<0.01, RF vs. IM).

(J) Sniffing duration towards each stimulus (seconds) during RF (red) vs. IM(blue) preference tests with saline and CNO injection. (Mean ± SEM, n = 6 Main effect of stimulus, **; p<0.01, RF vs. IM).

(K) Mean KDE probability of Z > 1 GCaMP7f signals obtained by summarizing KDE scores in each contact area in RF (red) vs. IM (blue) preference tests (Mean ± SEM, n = 6 Main effect of stimulus, ***; $p<0.001$, RF vs. IM) .

(L) Visualization of KDE shown in a virtual test environment (RF: top right corner, IM: bottom left corner). KDE was derived from body positions (green, left) and positions with Z > 1 GCaMP7f signals (red, right) recorded in 6 animals. The upper row represents KDE during saline injection, and the bottom row represents KDE during CNO injection.

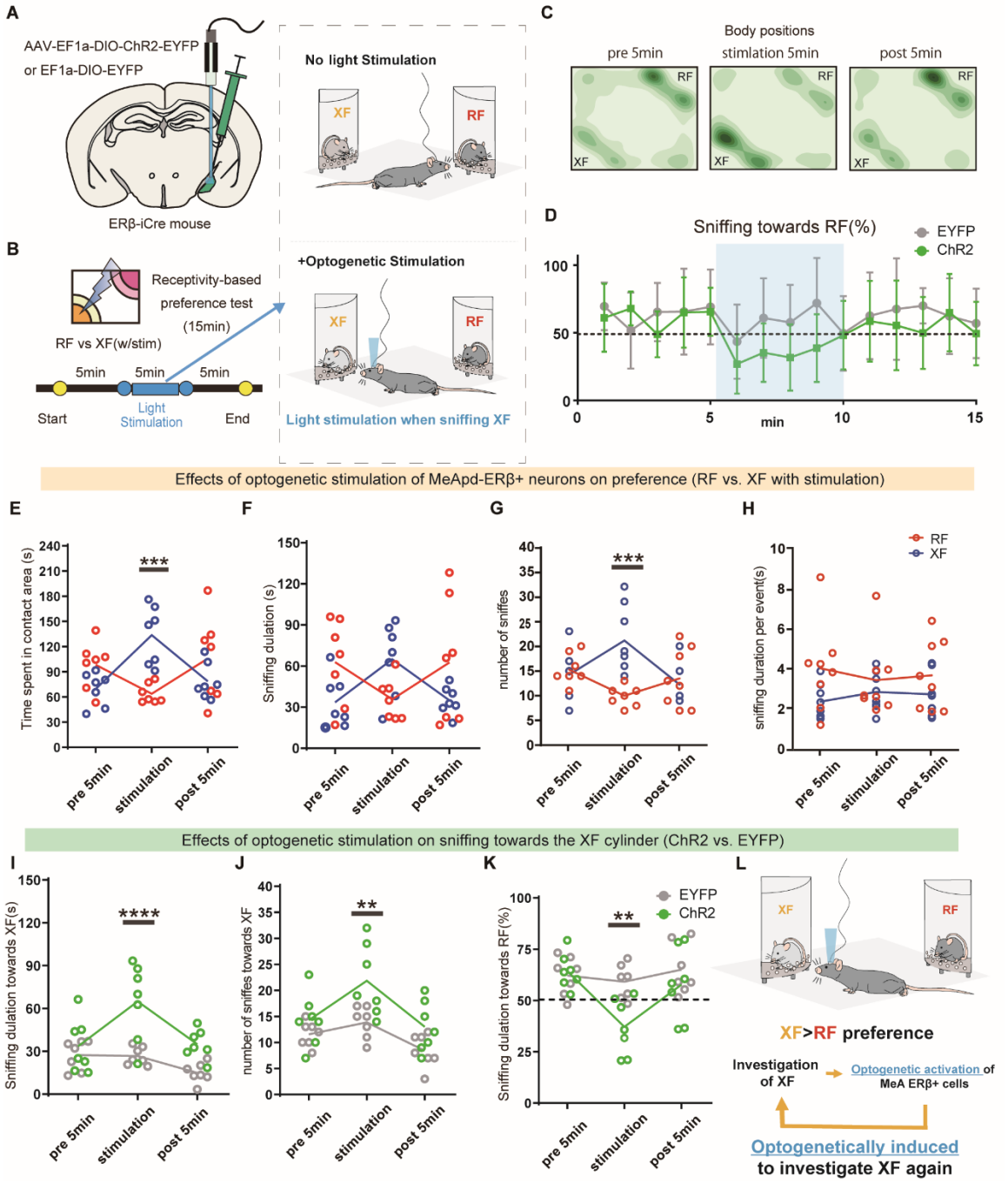
A
AAV-EF1a-DIO-ChR2-EYFP
or EF1a-DIO-EYFP
ERβ-iCre mouse
No light Stimulation
XF
RF
+Optogenetic Stimulation
Light stimulation when sniffing XF
B
Receptivity-based
preference test
(15min)
RF vs XF(w/stim)
5min
5min
5min
Start
Light
Stimulation
End
C
Body positions
pre 5min
stimlation 5min
post 5min
D
Sniffing towards RF(%)
EYFP
ChR2
min
Effects of optogenetic stimulation of MeApd-ERβ+ neurons on preference (RF vs. XF with stimulation)
E
Time spent in contact area (s)
F
Sniffing dulation (s)
G
number of sniffes
H
sniffing duration per event(s)
pre 5min
stimulation
post 5min
Effects of optogenetic stimulation on sniffing towards the XF cylinder (ChR2 vs. EYFP)
I
Sniffing dulation towards XF(s)
J
number of sniffes towards XF
K
Sniffing dulation towards RF(%)
L
XF>RF preference
Investigation
of XF
Optogenetic activation of
MeA ERβ+ cells
Optogenetically induced
to investigate XF again

Figure S6. Figures for Supplemental Study: Effects of optogenetic stimulation of MeApd-ERβ^{+} neurons on the levels of sniffing behavior

(A) Schematic diagram of AAV injection and fiber implantation in the MeApd for optogenetic stimulation study.

(B) Schematic diagram and timeline for the optogenetic stimulation study. Male mice were introduced into a receptivity-based (RF vs. XF) preference test environment for 15 minutes. Each test was divided into three 5-minute blocks (pre-stimulation, stimulation, and post-stimulation). Optical stimulation was delivered manually during the stimulation block while the animal was sniffing XF.

(C) Mean heat map presentation of body positions of male mice during pre-stimulation (left), stimulation (middle), and post-stimulation (right) 5-minute blocks.

(D) Mean percentage (%) of time sniffing towards the RF cylinder in each minute during RF vs. XF tests for the EYFP control (gray) and ChR2 (green) groups. The blue shaded area indicates the stimulation block (Mean ± SEM, n = 7 for EYFP and n=7 for ChR2).

(E) Mean time spent in the contact area (seconds) in each 5-minute block during RF (red) vs. XF (blue) preference tests (Mean ± SEM, n = 7, ***; $p<0.001$, RF vs. XF during the stimulation block).

(F) Mean sniffing duration (seconds) in each 5-minute block during RF (red) vs. XF (blue) tests (Mean ± SEM, n = 7).

(G) Mean number of sniffing events in each 5-minute block during RF(red) vs. XF(blue) tests (Mean ± SEM, n = 7, ***; $p<0.001$, RF vs. XF during the stimulation block).

(H) Mean sniffing duration per sniffing event in each 5-minute block during RF(red) vs. XF(blue) tests (Mean ± SEM, n = 7).

(I) Mean duration of sniffing (seconds) towards the XF cylinder in each 5-minute block during RF vs. XF tests for the EYFP control (gray) and ChR2 (green) groups (Mean ± SEM, n = 7 for EYFP and n=7 for ChR2, ****; $p<0.o001$, ChR2 vs. EYFP during the stimulation block).

(J) Mean number of sniffing events towards the XF cylinder in each 5-minute block during RF vs. XF tests for the EYFP control (gray) and ChR2 (green) groups (Mean ± SEM, n = 7 for EYFP and n=7 for ChR2, **; $p<0.01$, ChR2 vs. EYFP during the stimulation block).

(K) Mean percentage (%) of sniffing duration towards the RF cylinder in each 5-minute block during RF vs. XF tests for the EYFP control (gray) and ChR2 (green) groups (Mean ± SEM, n = 7 for EYFP and n=7 for ChR2, **; $p<0.01$, ChR2 vs. EYFP during the stimulation block).

(L) Schematic diagram demonstrating possible mechanisms of sniffing and preference to RF (vs. XF) induced by MeApd-ERβ^{+} neuronal excitation.

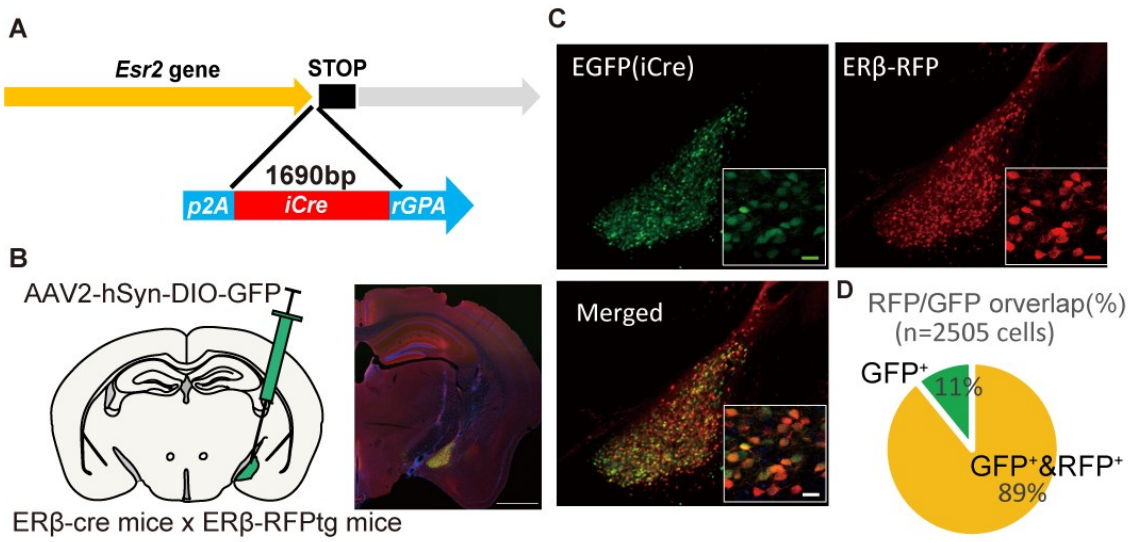

Figure S7. Generation and verification of ERβ-iCre mice

(A)Schematic diagram for generation of ERβ-iCre mice using CRISPR-Cas9. The 2A-iCre-rGPA sequence was knocked in right before the Stop codon of *Esr2* gene.

(B)Schematic diagram of AAV injection for Cre-dependent induction of GFP to the MeA in ERβ-iCre and ERβ-RFPtg double positive mice (left). EGFP and RFP expressing cells were localized in the MeApd (right), (Scale bar = 1 mm).

(C)Representative high magnification images showing iCre-dependently induced EGFP positive cells (top left), ERβ-RFP positive cells (top right), and merged image (bottom) in the MeApd (Scale bar = 10 μm).

(D)Percentage of RFP and EGFP co-expressing cells out of a total of 2505 EGFP positive cells (accumulated data from 3 mice) in the MeApd.

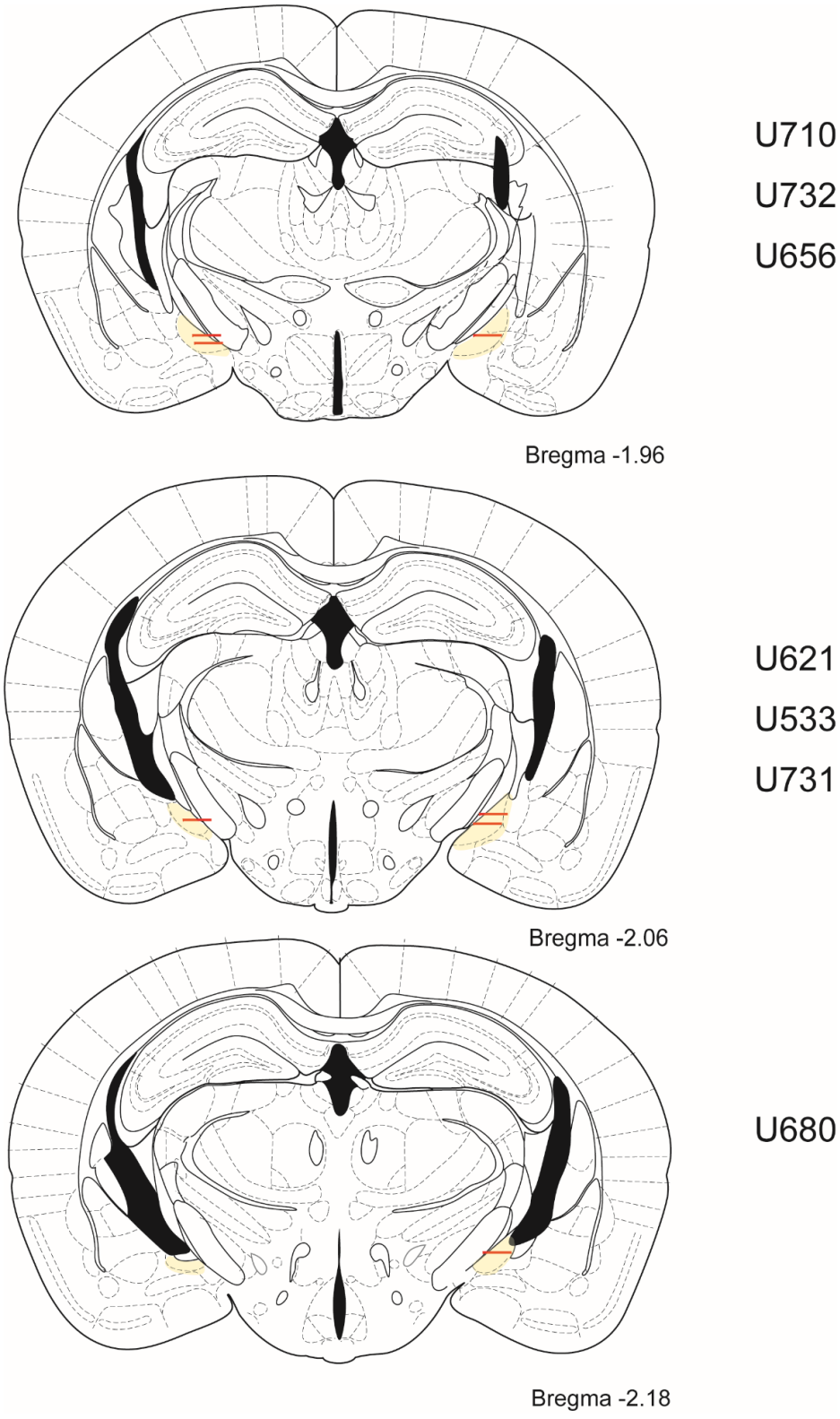

Figure S8. Fiber insertion sites for animals used in Study 1.

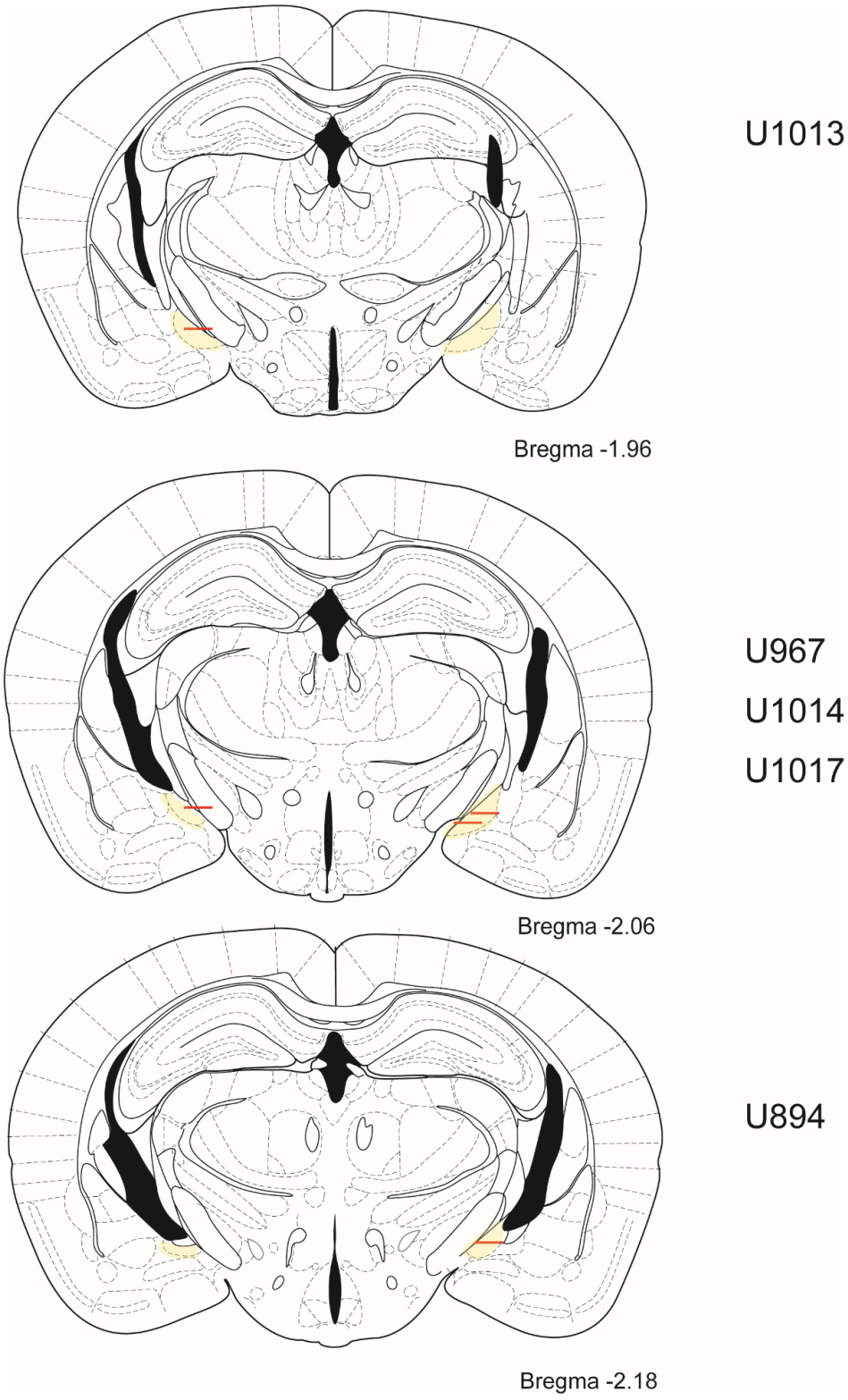

Figure S9. Fiber insertion sites for animals used in Study 2.

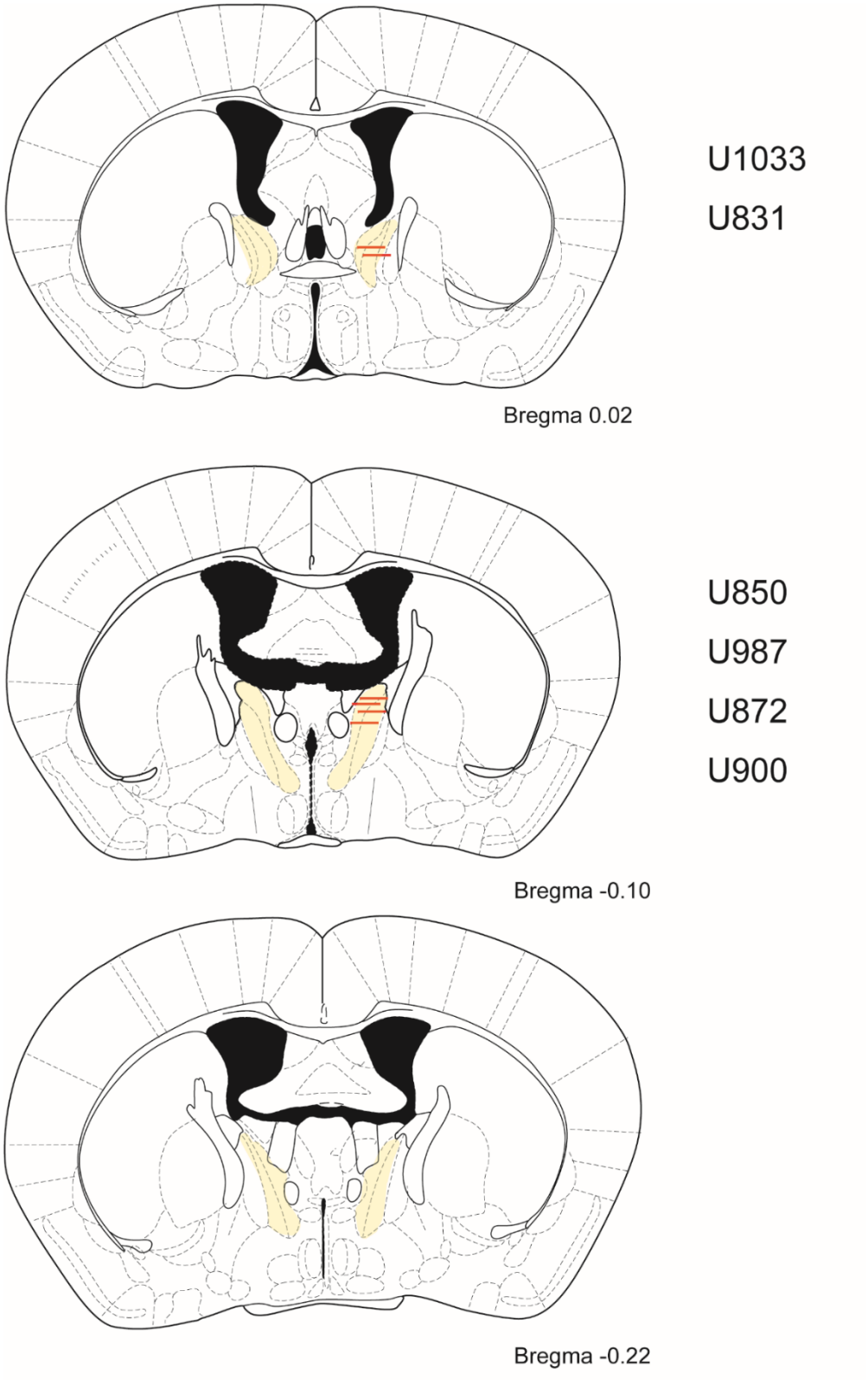

Figure S10. Fiber insertion sites for animals used in Study 4.

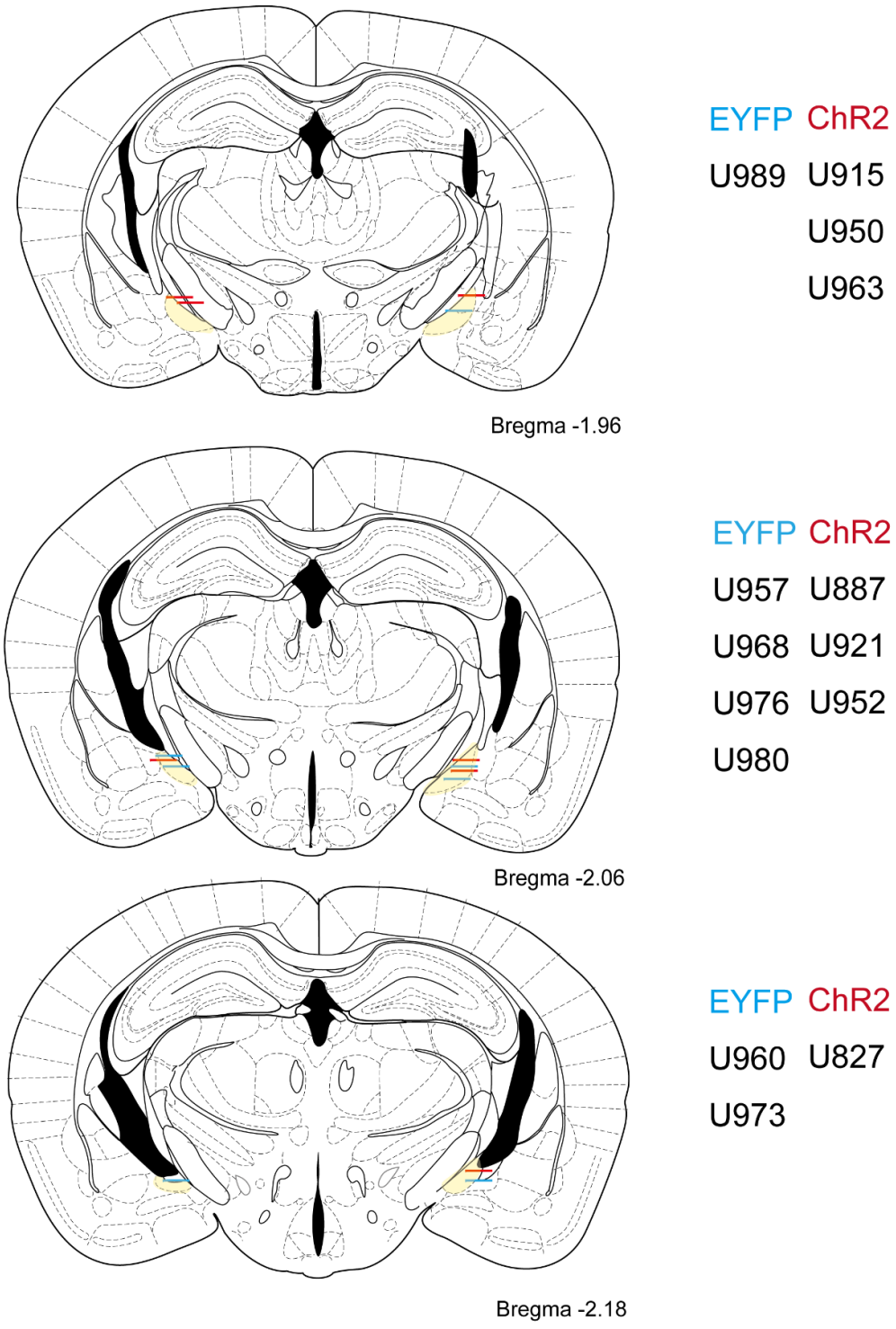

Figure S11. Fiber insertion sites for animals used in Supplemental Study.

Supplemental Movie. Representative fiber photometry recoding of MeApd-ERβ^{+} neuronal activity during a receptivity-based (RF vs. XF) preference test (60 seconds)

Top: Video recording of the behavior of a male mouse during a RF (bottom left) vs. XF (upper right) preference test.
Bottom: Fiber photometry recoding of ΔF/Fn neuronal activity (%) of MeApd-ERβ^{+} neurons with behavior annotations. Sniffing towards the RF and the XF cylinders is indicated with a background color of red and orange, respectively.

Supplemental references

1. G. R. Terrell, D. W. Scott, Variable Kernel Density Estimation. *Ann. Stat.* **20**, 1236–1265 (1992).

2. Y. Hasegawa, *et al.*, Generation of CRISPR/Cas9-mediated bicistronic knock-in *ins1-cre* driver mice. *Exp. Anim.* **65**, 319–327 (2016).

3. J. G. Lemmen, *et al.*, Expression of estrogen receptor alpha and beta during mouse embryogenesis. *Mech. Dev.* **81**, 163–167 (1999).

4. X. Fan, M. Warner, J.-Å. Gustafsson, Estrogen receptor β expression in the embryonic brain regulates development of calretinin-immunoreactive GABAergic interneurons. *Proc. Natl. Acad. Sci.* **103**, 19338–19343 (2006).

5. S. Sagoshi, *et al.*, Detection and Characterization of Estrogen Receptor Beta Expression in the Brain with Newly Developed Transgenic Mice. *Neuroscience* **438**, 182–197 (2020).

6. , Paxinos and Franklin's the Mouse Brain in Stereotaxic Coordinates - 5th Edition (April 12, 2023).

7. M. C. Tsuda, S. Ogawa, Long-Lasting Consequences of Neonatal Maternal Separation on Social Behaviors in Ovariectomized Female Mice. *PLOS ONE* **7**, e33028 (2012).

8. M. Nakata, *et al.*, Effects of Prepubertal or Adult Site-Specific Knockdown of Estrogen Receptor β in the Medial Preoptic Area and Medial Amygdala on Social Behaviors in Male Mice. *eNeuro* **3**, ENEURO.0155-15.2016 (2016).

9. O. Friard, M. Gamba, BORIS: a free, versatile open-source event-logging software for video/audio coding and live observations. *Methods Ecol. Evol.* **7**, 1325–1330 (2016).

10. A. Mathis, *et al.*, DeepLabCut: markerless pose estimation of user-defined body parts with deep learning. *Nat. Neurosci.* **21**, 1281–1289 (2018).

11. , GuPPy, a Python toolbox for the analysis of fiber photometry data | Scientific Reports (August 8, 2023).

12. N. Otsu, A Threshold Selection Method from Gray-Level Histograms. *IEEE Trans. Syst. Man Cybern.* **9**, 62–66 (1979).